Volume 2

Chapter 8

Detrital U–Pb Provenance, Mineralogy, and Geochemistry of the Cretaceous Colombian Back–Arc Basin

https://doi.org/10.32685/pub.esp.36.2019.08
Published online 25 November 2020

Javier GUERRERO[1]*, Alejandra MEJÍA–MOLINA[2], and José OSORNO[3]

1 jguerrerod@unal.edu.co
Universidad Nacional de Colombia
Sede Bogotá
Departamento de Geociencias
Carrera 30 n.° 45–03
Bogotá, Colombia

2 amejia@yachaytech.edu.ec
Universidad Yachay Tech
Hacienda Urcuquí s/n y Proyecto Yachay
Urcuquí, Ecuador

3 jose.osorno@anh.gov.co
Agencia Nacional de Hidrocarburos
Calle 26 n.° 59–65, segundo piso
Bogotá, Colombia

* Corresponding author

Supplementary Information:

S: https://www2.sgc.gov.co/LibroGeologiaColombia/tgc/sgcpubesp36201908s.pdf

Abstract The geology of the Cretaceous Colombian back–arc basin is reviewed considering detrital U–Pb provenance ages, mineralogy, and geochemistry of samples collected from outcrop sections and wells at several localities in the core of the Eastern Cordillera, Middle Magdalena Valley, and Catatumbo areas. The data set supports previous studies indicating a basin with main grabens in the present–day Eastern Cordillera between the Guaicáramo/Pajarito and Bituima/La Salina border faults, which operated as normal faults during the Cretaceous. Limestones are common on the western and northern sides of the basin, whereas terrigenous strata predominate on the eastern and southern sides. After the Berriasian, grabens were connected by marine flooding during the Valanginian, with two main source areas documented by distinct element and mineral contents, one in the Central Cordillera magmatic arc and the other in the Guiana Shield. Some elements present in Lower Cretaceous shales, including scandium, vanadium, and beryllium, are not related to the sediment supply areas for the basin but instead are linked to Valanginian to Cenomanian hydrothermal activity and dikes of gabbro, diorite, and tonalite emplaced during the main phase of extension in the basin.

Keywords: *Cretaceous, back–arc, Colombia, U–Pb provenance, geochemistry.*

Resumen La geología de la Cuenca Cretácica Colombiana de back–arc se revisa considerando edades de procedencia U–Pb, mineralogía y geoquímica de muestras colectadas en secciones de afloramientos y pozos de varias localidades en el núcleo de la cordillera Oriental, Valle Medio del Magdalena y Catatumbo. El conjunto de datos respalda estudios previos que indican una cuenca cuyos principales grábenes se encontraban en la cordillera Oriental actual, entre las fallas de Guaicáramo/Pajarito y Bituima/La Salina, que durante el Cretácico fueron fallas normales. Las calizas son comunes en los lados occidental y norte de la cuenca, mientras que los estratos terrígenos predominan en el lado este y sur de la misma. Después que los grábenes berriasianos de la cuenca se conectaron por inundación marina durante el Valanginiano, se pueden documentar dos áreas fuente con elementos y minerales distintivos, una en el arco magmático de la cordillera Central y otra en el Escudo de Guayana. Algunos elementos presentes en los *shales* del Cretácico Inferior, incluidos escandio, vanadio y berilio, no están relacionados con las áreas de aporte de los sedimentos de la cuenca,

Citation: Guerrero, J., Mejía–Molina, A. & Osorno, J. 2020. Detrital U–Pb provenance, mineralogy, and geochemistry of the Cretaceous Colombian back–arc basin. In: Gómez, J. & Pinilla–Pachon, A.O. (editors), The Geology of Colombia, Volume 2 Mesozoic. Servicio Geológico Colombiano, Publicaciones Geológicas Especiales 36, p. 261–297. Bogotá. https://doi.org/10.32685/pub.esp.36.2019.08

sino que están ligados con la actividad hidrotermal relacionada a los diques de gabro, diorita y tonalita, emplazados durante la extensión principal de la cuenca desde el Valanginiano hasta el Cenomaniano.

Palabras clave: *Cretácico, back–arc, Colombia, procedencia U–Pb, geoquímica.*

1. Introduction

The main depocenter of the Cretaceous Colombian back–arc basin is located in the present–day Eastern Cordillera, including the Cundinamarca, Boyacá, and Santander Departments, where several stratigraphic wells, oil wells, and field sections were studied (Figure 1). These areas include the Eastern Emerald Belt (Cinturón Esmeraldífero Oriental "CEOR"), Western Emerald Belt (Cinturón Esmeraldífero Occidental "CEOC"), Villeta, and Barichara/Bucaramanga. Three localities outside the main depocenter were also studied, including the Catatumbo area on the NE side of the basin and the Infantas oil well and Aguachica area (Middle Magdalena Valle "MMV") on the NW side of the basin.

The paleogeography and tectonic setting of the basin were initially documented using field–measured sections, sedimentary petrography, grain size distribution, and sequence stratigraphy (Guerrero, 2002a, 2002b; Guerrero et al., 2000). The presence of a magmatic arc delineating the western border of the basin during the entire Cretaceous Period is demonstrated using petrographic evidence that documents volcanic and metamorphic particles sourced from the Central Cordillera (Guerrero et al., 2000). Sandstones and biosparites have coarser grain sizes (very coarse to conglomeratic) along the eastern and western margins of the basin, where the thicknesses of coarse–grained units may reach hundreds of meters; these facies change gradually to finer–grained strata toward the center of the basin (Figures 2–4). Offshore biomicrites, marls, and shales are thicker toward the basin center, where they reach thicknesses of hundreds of meters.

Terrigenous sandstones and sandy biosparites on the western margin are volcanic and metamorphic litharenites sourced from the Central Cordillera; sandstones on the eastern basin margin are quartz arenites sourced mostly from recycled Paleozoic and older strata from the Guiana Shield. In fact, most Cretaceous sections rest in angular unconformity on Paleozoic strata along the eastern basin margin, whereas on the opposite, western margin of the basin, they rest in angular unconformity on Jurassic rocks. There is no sedimentological or structural continuity between Upper Jurassic and Lower Cretaceous strata in any place throughout the present–day Eastern Cordillera, so that there is not a continuous "Mesozoic basin". The basal sandstones of the Cretaceous system exposed near Girón and Zapatoca, which rest in angular unconformity on older basement and are transitionally covered by genetically related marine strata, were originally included in the Girón strata by Hettner (1892). Later, these beds were erroneously assigned to the Jurassic, based only on stratigraphic position, but in fact, they correspond to fluvial and shoreface transgressive sandstones of Berriasian and Valanginian age, which are now included in the Tambor, Tibasosa, Arcabuco, Buenavista, and Batá Formations (e.g., Etayo–Serna et al., 2003). There is no temporal or structural relationship between the basin and the Jurassic separation of Pangea, which affected parts of Brasil and Venezuela in northern South America. Actually, the Jurassic strata and igneous rocks, parallel to the Central Cordillera, are associated with a magmatic arc related to subduction along the western border of the continent (e.g., Bustamante et al., 2010; Zapata et al., 2016). The Cretaceous back–arc and forearc basins are also related to subduction of the Pacific Oceanic Plate beneath the western margin of South America. The Cretaceous succession from the Eastern Cordillera of Colombia was deposited in a back–arc basin related to subduction instead of a Mesozoic rift related to the breakup of Pangea. The Cretaceous strata that rest in angular unconformity on previously accreted oceanic crust in the Western Cordillera and on the western side of the Central Cordillera are assigned to the forearc basin and are not included in this study.

The main back–arc basin rift exposed in the Eastern Cordillera was controlled by NNE–striking normal faults that were active throughout the Cretaceous, as indicated by the great thickness (5000 m) and wide age range (Berriasian to Maastrichtian) of strata W of the Guaicáramo Fault compared to the reduced thickness (500 m) and restricted age range (only Turonian to Maastrichtian) of strata E of the fault (Guerrero, 2002b). After the Berriasian to Cenomanian synrift stage, subsidence continued to be greater in the central rift than in areas E of the Guaicáramo Fault, as indicated by the reduced thickness (ca. 500 m) of Turonian to Maastrichtian strata in the present–day Llanos Foothills and Putumayo areas compared to the approximately 1500 m of equivalent strata (Chipaque Formation, Guadalupe Group, and Guaduas Formation) W of the fault (Guerrero, 2002b; Guerrero & Sarmiento, 1996). Other evidence that supports the age of synrift subsidence is the presence of Valanginian to Cenomanian dikes of gabbro, diorite, and tonalite (Gómez

→

Figure 1. Study area in part of the Cretaceous Colombian back–arc basin, including the locations of wells and field sections from the CEOR (GA, MSP), Villeta (QP, RC), CEOC (BB, O), Barichara (QLP, QAD), Aguachica (CAB, CES), and Catatumbo (QLL, RR). The highest contents of zirconium (average percentages per locality) are in the SE part of the basin.

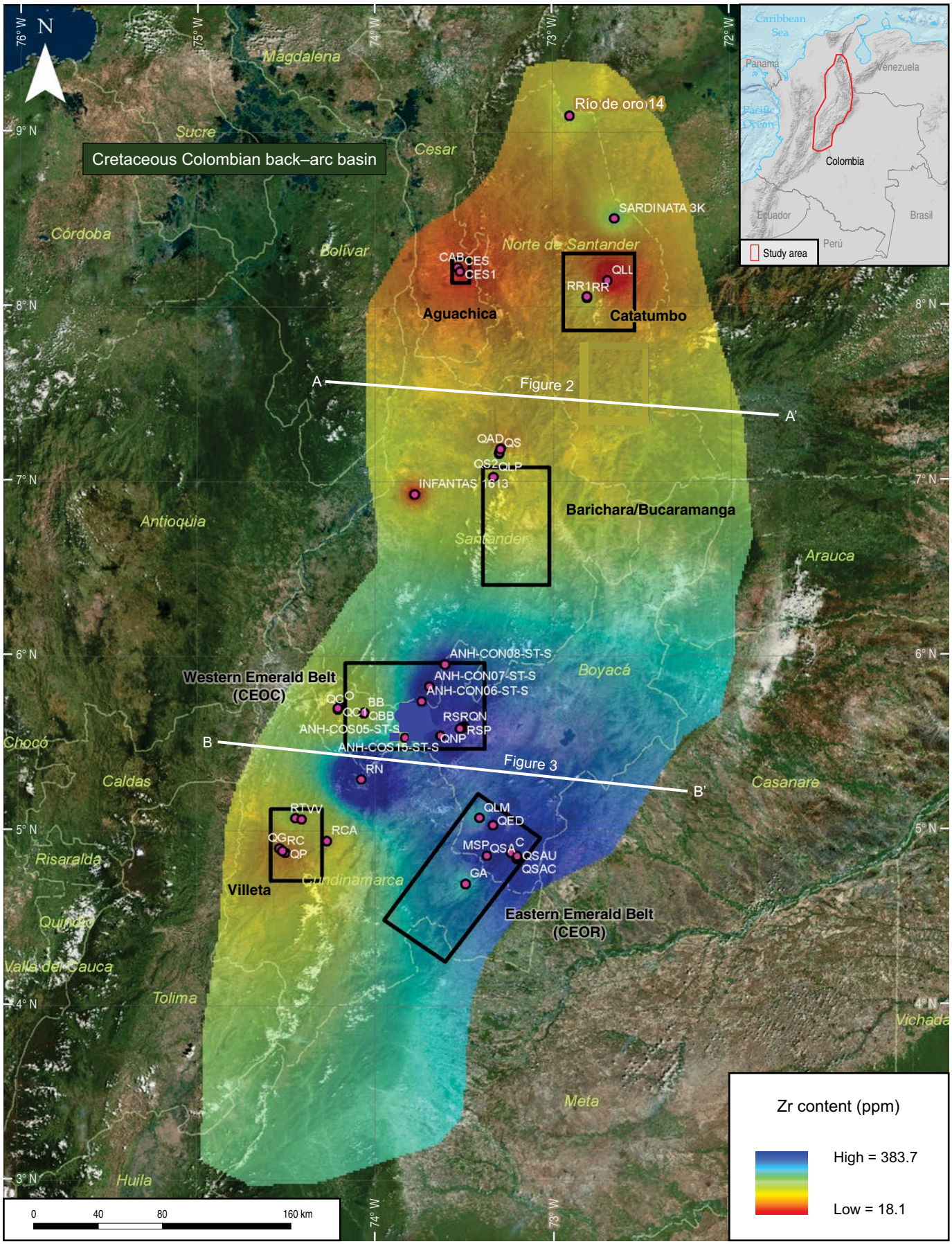
Cretaceous Colombian back–arc basin
Río de oro 14
SARDINATA 3K
Aguachica
Catatumbo
Barichara/Bucaramanga
Western Emerald Belt (CEOC)
Eastern Emerald Belt (CEOR)
Villeta
Figure 2
Figure 3
A
A'
B
B'
Magdalena
Sucre
Cesar
Córdoba
Bolívar
Norte de Santander
Antioquia
Santander
Arauca
Boyacá
Chocó
Caldas
Casanare
Risaralda
Cundinamarca
Quindío
Valle del Cauca
Tolima
Meta
Huila
Vichada
Caribbean Sea
Panamá
Venezuela
Pacific Ocean
Colombia
Ecuador
Brasil
Perú
Study area
Zr content (ppm)
High = 383.7
Low = 18.1
0
40
80
160 km

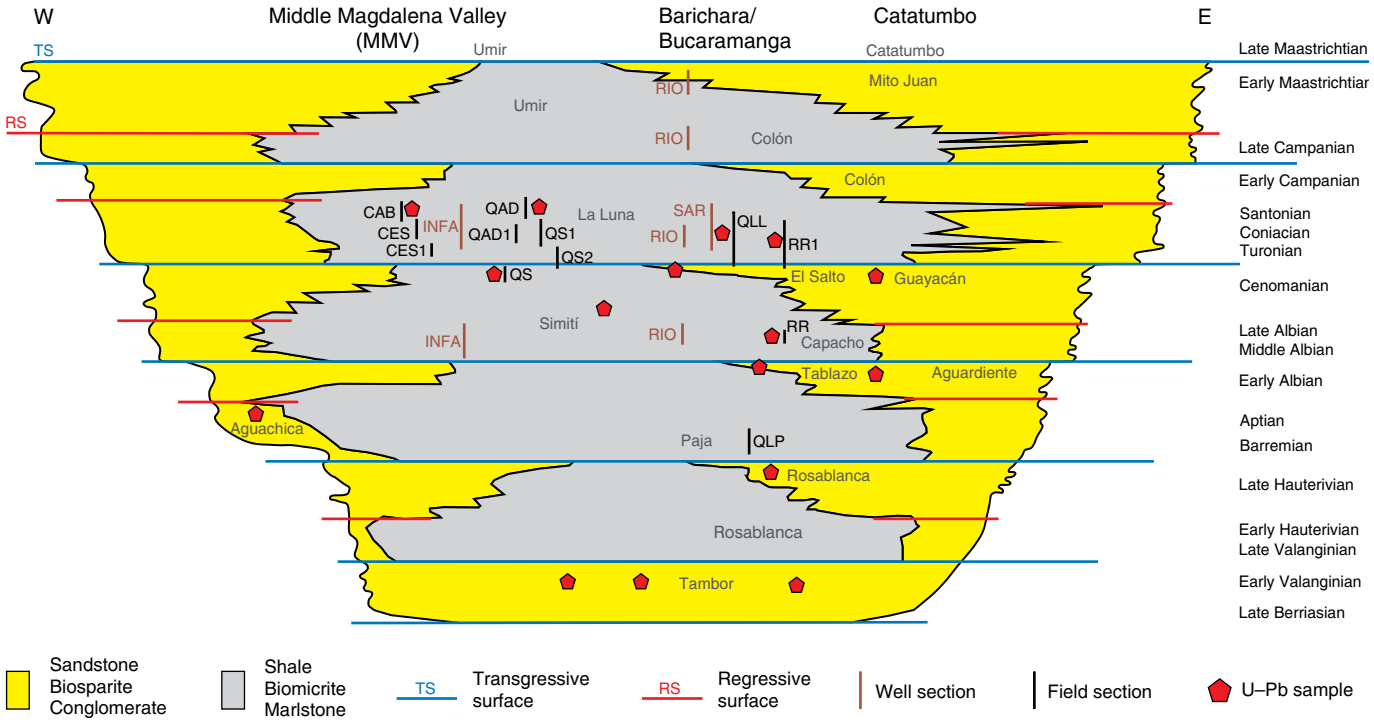

Figure 2. Units studied in the N sector of the basin, including the MMV, Barichara/Bucaramanga, and Catatumbo areas. Locations projected to line AA' of Figure 1 are: (CAB) Caño Agua Blanca; (CES) Caño El Salto; (QAD) Aguadulce Creek; (QS) La Sorda Creek; (QLL) La Leche Creek; (RR) Riecito River; (QLP) La Paja Creek. Oil wells are (INFA) Infantas; (RIO) Río de Oro; (SAR) Sardinata. Cross section modified from Guerrero (2002a).

et al., 2015; Vásquez et al., 2005, 2010), which intruded Lower Cretaceous strata during the main extensional phase of the basin. Subsequently, during the Turonian to Maastrichtian thermal subsidence of the basin, magmatic and hydrothermal activity stopped in the central rift.

The main rift was initially subdivided into grabens separated during the Berriasian but connected by the late Valanginian when the present–day Santander, Floresta, and Quetame Massifs were completely flooded by offshore marine strata. The role of Cretaceous normal faults and their Cenozoic inversion was initially discussed by Cooper et al. (1995) and has been recognized by Sarmiento–Rojas et al. (2006), Horton et al. (2010), and Mora et al. (2010), and among others. Tesón et al. (2013) documented several grabens, including Guatiquía, Pisba, Cocuy, and Tablazo, which were bounded by the Guaicáramo, Pajarito, Pesca, Servitá, Lengupá, Soapaga, Boyacá, Bituima, and La Salina normal faults.

The purposes of this chapter are to better document the two source areas and the evolution of the Cretaceous Colombian back–arc basin and to characterize the rock types from successions at several localities. We present new results on XRD mineralogy and ICP–MS/OES geochemistry mainly from shales and biomicrites, along with U–Pb ages of zircon grains contained in sandstones from both sides of the basin.

2. Materials and Methods

Fine–grained strata including biomicrites, marls, and shales, as well as coarse–grained strata including sandstones and biosparites, were collected mainly from 9 wells and 35 field sections of key localities within the basin (Figures 1–4; Tables 1–3). Table 1 contains the initial and final coordinates of stratigraphic sections exposed along creeks, rivers, and roads. Table 2 displays the coordinates of sampled oil and stratigraphic wells, with the depth information in feet for each unit. Table 3 contains the stratigraphic information and the coordinates of sandstone samples collected outside the main stratigraphic sections.

Selected samples of sandstone, volcanic tuff, and limestone were processed for detrital zircon U–Pb dating with a single collector quadrupole LA–ICP–MS Agilent 7700x instrument at the laboratories of Apatite to Zircon, Inc., in Viola, Idaho, USA. Details of the procedures, statistics, and standards employed are presented by Chew & Donelick (2012), Moore (2014), and Moore et al. (2015). According to the report provided by Apatite to Zircon, Inc., the approach was the modeling of background–corrected signal intensities for each isotope in each scan. U–Pb age standards for which independently accepted ages are published were designated primary, secondary, and tertiary for purposes of age calibration. A minimum of

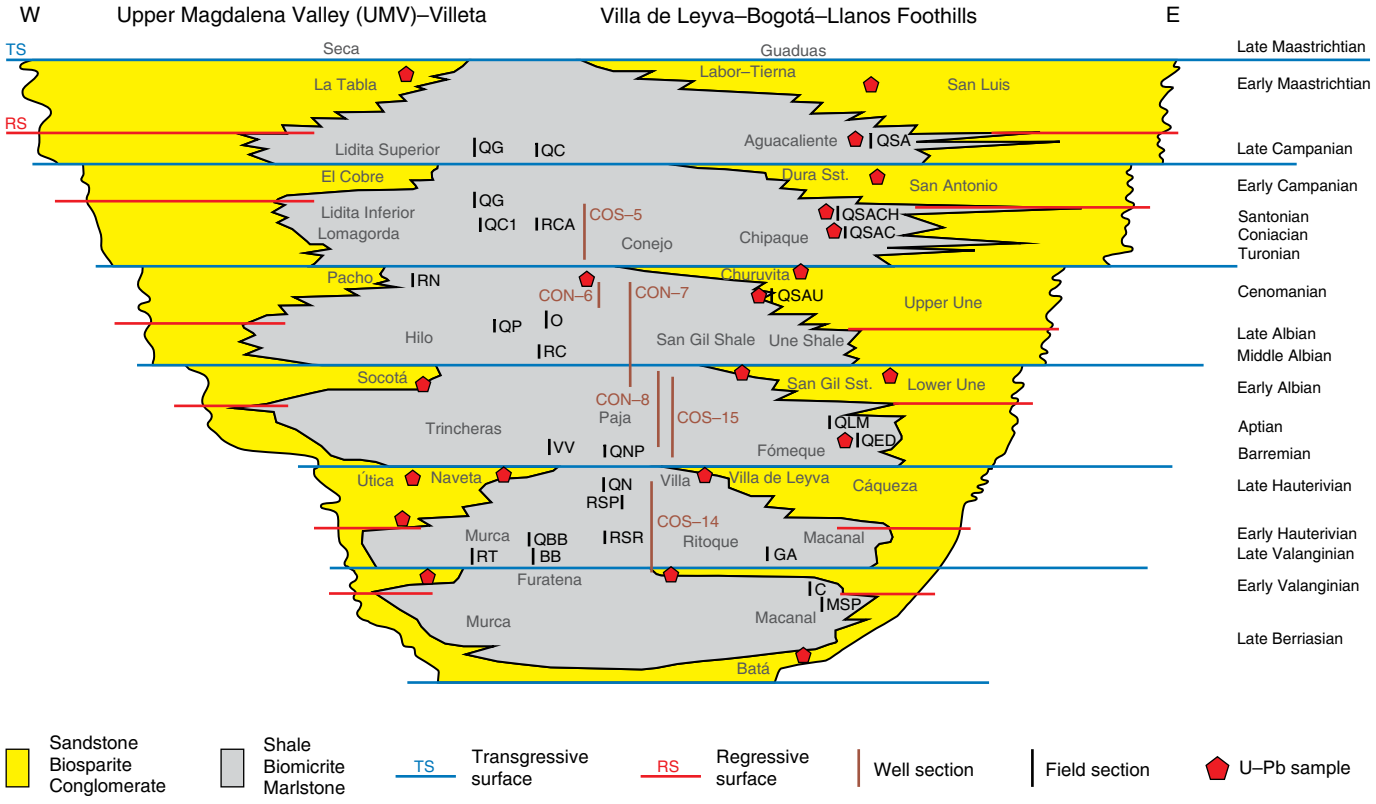

Figure 3. Units studied in the S sector of the basin. Locations projected to line BB' of Figure 1. Sections are from (R) rivers; (Q) creeks; and road cuts, including (MSP) San Pedro Mine; (C) Cachipay; (GA) Gachalá; (RT) Tobia River; (QBB) Buriburi Creek; (RS) Samacá River; (QN) Negra Creek; (VV) Caiquero; (QED) El Dátil Creek; (QLM) Los Monos Creek; (QSA) San Antonio Creek; (RC) Contador River; (QP) Piñal Creek; (O) Otanche; (RN) Negro River; (QC) Cobre Creek; (RCA) Cañas River; (QG) Guate Creek. Stratigraphic Agencia Nacional de Hidrocarburos (ANH) wells are COS–14, COS–15, CON–8, CON–7, CON–6, and COS–5. Cross–section modified from Guerrero (2002a).

two primary and two secondary standard spots were analyzed prior to and following each group of ca. 25–40 tertiary standards and/or unknown sample spots. Tertiary standards were also analyzed with the primary and secondary standards. For a particular isotopic ratio (e.g., $^{206}Pb/^{238}U$), the fractionation factor equals the accepted isotopic ratio divided by the measured ratio (radiogenic Pb only). For zircon U–Pb standards, common Pb was assumed to be negligible, and fractionation factors and their absolute errors were determined directly for the isotopes of interest. Fractionation factors and their errors for each spot were smoothed to yield session–wide spot fractionation factors and their errors. Fractionation factors were calculated based on the following assumptions: (a) ^{235}U values were calculated from measured ^{238}U values (Steiger & Jäger, 1977) and (b) zero fractionation was assumed between ^{206}Pb and ^{207}Pb. For common Pb correction, the Stacey & Kramers (1975) common Pb model for the Earth was used. Ages and common Pb ratios were determined iteratively using an arbitrary, session–wide minimum common Pb age value (the default minimum common Pb age was arbitrarily set equal to the age of the oldest age standard in the current session). For each scan, U–Pb ages and their asymmetrical errors were calculated. For a sum of N scans, the U–Pb age and its error were calculated from the sum of the respective isotopes and a fractionation factor calculated as a weighted sum of N fractionation factors, one fractionation factor for each scan, and each fractionation factor was weighted by the amount of uranium or thorium for the scan.

In total, 110 inclusion–free zircon grains were processed from most samples, obtaining an average of 100 dates per sample. The reported results consist of a single date for each analyzed zircon grain. Data are plotted as age histograms and age probability distribution functions. Detailed data are presented in Tables 1 and 2 of the Supplementary Information.

Heavy minerals were processed by HM Research Associates in St. Ishmaels, Pembrokeshire, UK. Elemental analyses were conducted at ACME Analytical Laboratories in Bogotá, Colombia, using a Thermo 6500 DUO equipment for ICP–OES of major elements and an Agilent 7500cx system for ICP–MS of minor elements and REE. Samples were previously fused with lithium borate salts using a Claisse M4 Fluxer.

3. Results

The results from U–Pb provenance analyses are displayed in Table 4 and Tables 1, 2 of the Supplementary Information. The youngest ages are in the interval of 50 to 150 Ma and corre-

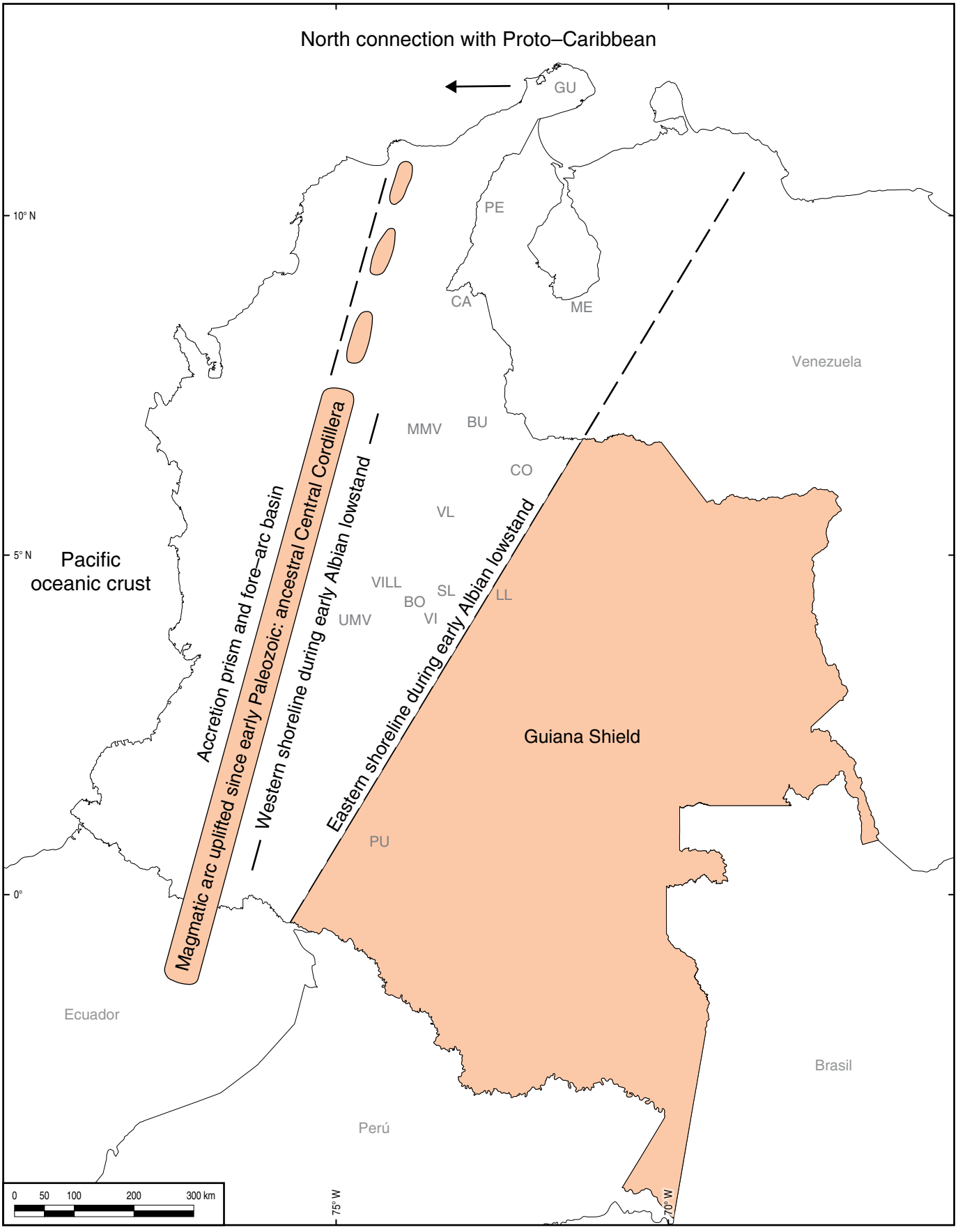
North connection with Proto–Caribbean
GU
PE
CA
ME
Venezuela
10° N
5° N
0°
MMV
BU
CO
VL
VILL
SL
LL
BO
VI
UMV
PU
Pacific
oceanic crust
Accretion prism and fore–arc basin
Magmatic arc uplifted since early Paleozoic: ancestral Central Cordillera
Western shoreline during early Albian lowstand
Eastern shoreline during early Albian lowstand
Guiana Shield
Ecuador
Perú
Brasil
0 50 100 200 300 km
75° W
70° W

Figure 4. Location of the Cretaceous Colombian back–arc basin between the Central Cordillera and the Guiana Shield. The studied sections include the CEOR (SL, VI); Villeta (VILL); CEOC/Villa de Leyva (VL); Barichara/Bucaramanga (BU); Aguachica (MMV); Catatumbo (CA). Referenced sections include: (PU) Putumayo; (UMV) Upper Magdalena Valley; (LL) Llanos; (BO) Bogotá; (CO) Cocuy; (PE) Périja; (ME) Mérida. La Guajira Peninsula (GU) was aligned with the Santa Marta Massif and the Central Cordillera. Modified from Guerrero (2002a) and Guerrero et al. (2000).

spond to coeval Cretaceous particles present in strata from the Magdalena Valley and W side of the Eastern Cordillera. Important age peaks of 150 to 200 Ma (Jurassic) and 200 to 250 (Triassic) are also present on the W side of the basin.

Older peaks, present in samples from both the E and W sides of the study area, are centered around 250 to 550 Ma (Paleozoic) and 900 to 1200 Ma (late Mesoproterozoic to early Neoproterozoic); however, these ages are more common in samples from the E side of the Eastern Cordillera. Other important provenance ages are around 1500 Ma (early Mesoproterozoic) and 1800 Ma (late Paleoproterozoic), which are also more common on the E side of the Eastern Cordillera. The oldest grains, 3250 to 3950 Ma (Paleoarchean and Eoarchean), are present in very minor amounts, usually 1 or 2 particles per sample.

XRD mineralogical results from selected units are displayed in Table 5. The highest contents of kaolinite and montmorillonite correspond mainly to the Llanos Foothills, CEOR, Villa de Leyva, and Barichara areas. The highest contents of illite and chlorite are mainly from the CEOC, Villeta, and Magdalena Valley areas. The percentages displayed are averages per formation in a particular section. The majority are field sections, except for wells COS–5, COS–14, COS–15, CON–6, CON–7, CON–8, SAR 3K, and INFA–1613. Most samples were processed from shales, but there are also marlstones, biomicrites, and cherts. The lowest clay mineral contents (1 to 5 %) are from biomicrites and cherts of La Luna Formation; the highest contents (69%) are from the Chipaque Formation shales. The last column reports the sum of phyllosilicates, including illite, pyrophyllite, kaolinite, chlorite, and montmorillonite.

ICP–OES major element percentages of selected shale beds are displayed in Table 6. Samples with the highest Al_2O_3 contents are mainly from units with high amounts of mudstone and clay shale, including the Paja, San Gil, Chipaque, Conejo, Fómeque, and Macanal Formations. In these units, most clay–sized particles correspond to clay minerals, as indicated by XRD analyses. Samples with the highest contents of titanium (COS–15–2054 Paja Formation), chromium (O–75 Hilo Formation), and scandium (C–12 Macanal Formation) are included.

The ICP–OES major element percentages of limestone and chert units (with less than 5% Al_2O_3) are displayed in Table 7. Samples with the highest CaO contents include mainly examples from La Luna Formation biomicrites. The highest SiO_2 contents correspond to diagenetic cherts of the Lidita Inferior, Lidita Superior, Hilo, and La Luna Formations. The samples with the highest contents of nickel (SAR–7443) and phosphorus (QLL–55) in the study are from La Luna Formation in the Catatumbo area.

Minor elements of selected biomicrite and shale units are presented in ppm in Table 8. The highest contents of vanadium are from shale samples (QP–440 and O–05) of the Hilo Formation from the Villeta and CEOC areas. The highest contents of uranium (SAR–7443) and strontium (QLL–55) are from biomicrite samples of La Luna Formation in the Catatumbo area. The highest values of scandium are from the Macanal (C–12 and MSP–25), Villa de Leyva (COS14–459), and Fómeque (QED–35) Formations. The highest zirconium value is from a sample (COS15–2054) of the Paja Formation in the Villa de Leyva area. The regional distribution of zirconium is also presented in Figure 1.

Table 9 presents the REE in ppm. The highest cerium content is present in a sample (COS14–1575) from the Arcabuco Formation in the Villa de Leyva area. High cerium values are present mostly in the Paja and San Gil Shales from the Villa de Leyva area, along with the Aguacaliente and Une Formations from the Llanos Foothills. The highest content of yttrium is from a sample (RT–10) of the Murca Formation in the Villeta area. The heavy REE are generally associated with the Murca, Trincheras, and Pacho Formations from the Villeta area.

4. Discussion

4.1. Provenance and Paleogeography of the Basin from Detrital Zircon U–Pb Ages

Zircon U–Pb dates obtained from samples collected at several stratigraphic positions and various localities (Figures 1–4) confirm previous paleogeographic reconstructions based on petrography and sandstone distribution (Guerrero, 2002a, 2002b; Guerrero et al., 2000), indicating a back–arc basin sourced from the magmatic arc in the W and the Guiana Shield in the E during the entire Cretaceous time span. Samples are mainly sandstones, but finer–grained strata, including a few siltstones, shales, and biomicrites, are included. Most formations were sampled several times, so a few representative examples are presented here to illustrate the source areas.

4.1.1. Llanos Foothills and CEOR

In the SE sector of the basin, along the periphery of Bogotá, Villavicencio, and San Luis, the Cretaceous succession and Paleozoic sedimentary basement were sampled. The youngest zircon particles in Paleozoic strata are 300 to 350 Ma (Figure 5), which confirms the Carboniferous age of the Farallones Group.

Table 1. Location of field sections.

Sample	Section	Area	Formation	Age	Latitude N	Longitude W
BB–00	Buriburi	CEOC	Furatena (Lower)	Berriasian – early Hauterivian	5° 40’ 28.931”	74° 03’ 54.439”
BB–10	Buriburi	CEOC	Furatena (Lower)	Berriasian – early Hauterivian	5° 40’ 27.833”	74° 03’ 53.743”
C–00	Cachipay	CEOR	Macanal	Berriasian – early Hauterivian	4° 52’ 24.791”	73° 14’ 18.525”
C–48	Cachipay	CEOR	Macanal	Berriasian – early Hauterivian	4° 52’ 23.458”	73° 14’ 16.868”
CAB–00	Agua Blanca Creek	Aguachica	La Luna (Upper)	Coniacian to Santonian	8° 13’ 28.226”	73° 32’ 07.428”
CAB–128	Agua Blanca Creek	Aguachica	La Luna (Upper)	Coniacian to Santonian	8° 13’ 25.764”	73° 32’ 11.248”
CAB–130	Agua Blanca Creek	Aguachica	Umir (Lower)	Early Campanian	8° 13’ 25.725”	73° 32’ 11.306”
CES–00	El Salto Creek	Aguachica	La Luna	Turonian to Santonian	8° 12’ 08.312”	73° 31’ 18.000”
CES–82	El Salto Creek	Aguachica	La Luna	Turonian to Santonian	8° 12’ 05.444”	73° 31’ 20.457”
CES1–00	El Salto Creek	Aguachica	La Luna	Turonian to Santonian	8° 12’ 08.911”	73° 31’ 13.229”
CES1–20	El Salto Creek	Aguachica	La Luna	Turonian to Santonian	8° 12’ 08.853”	73° 31’ 13.827”
GA–00	Gachalá	CEOR	Macanal	Berriasian – early Hauterivian	4° 41’ 44.416”	73° 29’ 43.044”
GA–62	Gachalá	CEOR	Macanal	Berriasian – early Hauterivian	4° 41’ 45.454”	73° 29’ 46.375”
MSP–00	M. San Pedro	CEOR	Macanal	Berriasian – early Hauterivian	4° 51’ 23.858”	73° 22’ 28.851”
MSP–36	M. San Pedro	CEOR	Macanal	Berriasian – early Hauterivian	4° 51’ 24.804”	73° 22’ 30.268”
O–00	Otanche	CEOC	Hilo	Middle and late Albian	5° 42’ 50.420”	74° 11’ 54.956”
O–96	Otanche	CEOC	Hilo	Middle and late Albian	5° 42’ 49.222”	74° 11’ 51.865”
QAD–00	Aguadulce Creek	Barichara	La Luna	Turonian to Santonian	7° 11’ 06.173”	73° 17’ 40.617”
QAD–77	Aguadulce Creek	Barichara	La Luna	Turonian to Santonian	7° 11’ 06.670”	73° 17’ 43.550”
QAD1–00	Aguadulce Creek 1	Barichara	La Luna	Turonian to Santonian	7° 11’ 18.134”	73° 17’ 32.182”
QAD1–60	Aguadulce Creek 1	Barichara	La Luna	Turonian to Santonian	7° 11’ 18.037”	73° 17’ 34.405”
QBB–00	Buriburi Creek	CEOC	Furatena (Lower)	Berriasian – early Hauterivian	5° 40’ 36.746”	74° 03’ 41.176”
QBB–12	Buriburi Creek	CEOC	Furatena (Lower)	Berriasian – early Hauterivian	5° 40’ 36.717”	74° 03’ 40.604”
QC–00	Cobre Creek	CEOC	Lidita Inferior	Late Santonian	5° 41’ 41.386”	74° 12’ 27.255”
QC–50	Cobre Creek	CEOC	Lidita Inferior	Late Santonian	5° 41’ 39.970”	74° 12’ 26.572”
QC1–00	Cobre Creek 1	CEOC	Lomagorda	Turonian to Santonian	5° 42’ 04.020”	74° 12’ 27.205”
QC1–54	Cobre Creek 1	CEOC	Lomagorda	Turonian to Santonian	5° 42’ 02.266”	74° 12’ 25.176”
QED–00	El Dátil Creek	CEOR	Fómeque	Barremian and Aptian	5° 01’ 54.296”	73° 20’ 25.292”
QED–36	El Dátil Creek	CEOR	Fómeque	Barremian and Aptian	5° 01’ 55.929”	73° 20’ 24.462”
QG–00	Guate Creek	Villeta	Lidita Inf.	Late Santonian	4° 53’ 59.292”	74° 32’ 03.307”
QG–137	Guate Creek	Villeta	Lidita Inf.	Late Santonian	4° 54’ 01.026”	74° 32’ 08.472”
QG–251	Guate Creek	Villeta	Lidita Sup.	Late Campanian	4° 54’ 00.408”	74° 32’ 13.807”
QG–292	Guate Creek	Villeta	Lidita Sup.	Late Campanian	4° 54’ 00.354”	74° 32’ 15.777”
QLL–00	La Leche Creek	Catatumbo	Guayacán	Cenomanian	8° 08’ 56.797”	72° 41’ 31.315”
QLL–02	La Leche Creek	Catatumbo	Guayacán	Cenomanian	8° 08’ 57.311”	72° 41’ 30.412”
QLL–04	La Leche Creek	Catatumbo	La Luna	Turonian to Santonian	8° 08’ 57.822”	72° 41’ 29.509”
QLL–63	La Leche Creek	Catatumbo	La Luna	Turonian to Santonian	8° 09’ 09.873”	72° 41’ 14.692”
QLM–00	Los Micos Creek	CEOR	Fómeque	Barremian and Aptian	5° 04’ 22.882”	73° 24’ 53.983”
QLM–53	Los Micos Creek	CEOR	Fómeque	Barremian and Aptian	5° 04’ 20.588”	73° 24’ 57.524”
QLP–00	La Paja Creek	Barichara	Paja	Barremian and Aptian	7° 01’ 26.468”	73° 20’ 04.444”
QLP–66	La Paja Creek	Barichara	Paja	Barremian and Aptian	7° 01’ 25.114”	73° 20’ 08.359”
QN–00	Negra Creek	CEOC	Villa de Leyva	Late Hauterivian	5° 35’ 40.402”	73° 30’ 02.088”

Table 1. Location of field sections (*continued*).

Sample	Section	Area	Formation	Age	Latitude N	Longitude W
QN–10	Negra Creek	CEOC	Villa de Leyva	Late Hauterivian	5° 35' 39.696"	73° 30' 02.193"
QNP–00	Negra Creek	CEOC	Paja	Barremian and Aptian	5° 35' 38.593"	73° 29' 56.222"
QNP–34	Negra Creek	CEOC	Paja	Barremian and Aptian	5° 35' 37.967"	73° 29' 54.923"
QP–00	Piñal Creek	Villeta	Hilo	Middle and late Albian	4° 52' 25.191"	74° 30' 09.671"
QP–465	Piñal Creek	Villeta	Hilo	Middle and late Albian	4° 52' 06.673"	74° 29' 55.123"
QS–00	La Sorda Creek	Barichara	El Salto	Cenomanian	7° 09' 38.294"	73° 18' 05.373"
QS–16	La Sorda Creek	Barichara	El Salto	Cenomanian	7° 09' 38.753"	73° 18' 05.597"
QS1–02	La Sorda Creek 1	Barichara	La Luna (Lower)	Turonian	7° 09' 50.411"	73° 18' 04.775"
QS1–36	La Sorda Creek 1	Barichara	La Luna (Lower)	Turonian	7° 09' 48.200"	73° 18' 06.301"
QS2–00	La Sorda Creek 2	Barichara	El Salto	Cenomanian	7° 09' 57.080"	73° 18' 00.931"
QS2–20	La Sorda Creek 2	Barichara	El Salto	Cenomanian	7° 09' 58.418"	73° 18' 01.340"
QS2–22	La Sorda Creek 2	Barichara	La Luna (Lower)	Turonian	7° 09' 58.552"	73° 18' 01.379"
QS2–52	La Sorda Creek 2	Barichara	La Luna (Lower)	Turonian	7° 10' 00.565"	73° 18' 01.991"
QSA–00	San Antonio Creek	CEOR	Aguacaliente	Late Campanian	4° 50' 15.031"	73° 12' 25.203"
QSA–100	San Antonio Creek	CEOR	Aguacaliente	Late Campanian	4° 50' 11.838"	73° 12' 25.178"
QSAC–00	S. Antonio Creek C	CEOR	Chipaque	Turonian to Santonian	4° 50' 34.658"	73° 12' 23.685"
QSAC–48	S. Antonio Creek C	CEOR	Chipaque	Turonian to Santonian	4° 50' 33.001"	73° 12' 23.408"
QSACH–00	S. Antonio Creek Ch	CEOR	Chipaque	Turonian to Santonian	4° 50' 27.921"	73° 12' 24.635"
QSACH–30	S. Antonio Creek Ch	CEOR	Chipaque	Turonian to Santonian	4° 50' 26.784"	73° 12' 24.231"
QSAU–00	S. Antonio Creek U	CEOR	Une (Upper)	Late Cenomanian	4° 51' 13.714"	73° 12' 14.776"
QSAU–18	S. Antonio Creek U	CEOR	Une (Upper)	Late Cenomanian	4° 51' 13.752"	73° 12' 14.292"
RC–00	Contador River	Villeta	Hilo (Lower)	Middle Albian	4° 52' 59.887"	74° 31' 09.813"
RC–44	Contador River	Villeta	Hilo (Lower)	Middle Albian	4° 52' 59.100"	74° 31' 08.615"
RCA–00	Cañas River	Villeta	Conejo	Turonian to Santonian	4° 56' 31.704"	74° 16' 10.733"
RCA–80	Cañas River	Villeta	Conejo	Turonian to Santonian	4° 56' 28.080"	74° 16' 02.777"
RN–00	Negro River	CEOC	Pacho	Cenomanian	5° 17' 35.949"	74° 04' 43.213"
RN–112	Negro River	CEOC	Pacho	Cenomanian	5° 17' 33.238"	74° 04' 52.281"
RR–02	Riecito River	Catatumbo	Capacho	Middle and late Albian	8° 03' 02.089"	72° 48' 26.230"
RR–20	Riecito River	Catatumbo	Capacho	Middle and late Albian	8° 03' 05.512"	72° 48' 26.056"
RR1–00	Riecito River 1	Catatumbo	Guayacán	Cenomanian	8° 03' 30.022"	72° 48' 26.355"
RR1–10	Riecito River 1	Catatumbo	Guayacán	Cenomanian	8° 03' 30.158"	72° 48' 27.350"
RR1–18	Riecito River 1	Catatumbo	La Luna	Turonian to Santonian	8° 03' 30.265"	72° 48' 28.150"
RR1–60	Riecito River 1	Catatumbo	La Luna	Turonian to Santonian	8° 03' 30.834"	72° 48' 32.337"
RSP–00	Samacá River	CEOC	Villa de Leyva	Late Hauterivian	5° 35' 19.005"	73° 30' 44.572"
RSP–32	Samacá River	CEOC	Villa de Leyva	Late Hauterivian	5° 35' 17.562"	73° 30' 43.650"
RSR–00	Samacá River	CEOC	Ritoque	Late Valanginian – early Hauterivian	5° 35' 30.385"	73° 30' 54.584"
RSR–34	Samacá River	CEOC	Ritoque	Late Valanginian – early Hauterivian	5° 35' 31.205"	73° 30' 51.049"
RT–00	Tobia River	Villeta	Murca (Lower)	Berriasian – early Hauterivian	5° 04' 16.218"	74° 26' 44.287"
RT–62	Tobia River	Villeta	Murca (Lower)	Berriasian – early Hauterivian	5° 04' 14.781"	74° 26' 40.134"
VV–00	Caiquero	Villeta	Trincheras	Barremian and Aptian	5° 03' 51.475"	74° 24' 41.054"
VV–89	Caiquero	Villeta	Trincheras	Barremian and Aptian	5° 03' 47.484"	74° 24' 32.936"

Table 2. Location of wells.

Sample and depth in feet	Well	Area	Formation	Age	Latitude N	Longitude W
CON–06–360	ANH–CON–06	CEOC	Churuvita	Cenomanian	5° 44' 26.202"	73° 44' 14.826"
CON–06–1470	ANH–CON–06	CEOC	Churuvita	Cenomanian	5° 44' 26.202"	73° 44' 14.826"
CON–07–134	ANH–CON–07	CEOC	Churuvita	Cenomanian	5° 49' 30.758"	73° 41' 47.587"
CON–07–240	ANH–CON–07	CEOC	Churuvita	Cenomanian	5° 49' 30.758"	73° 41' 47.587"
CON–07–485	ANH–CON–07	CEOC	San Gil Shale	Middle and late Albian	5° 49' 30.758"	73° 41' 47.587"
CON–07–1810	ANH–CON–07	CEOC	San Gil Shale	Middle and late Albian	5° 49' 30.758"	73° 41' 47.587"
CON–07–1880	ANH–CON–07	CEOC	San Gil Sandstone	Early Albian	5° 49' 30.758"	73° 41' 47.587"
CON–07–2420	ANH–CON–07	CEOC	San Gil Sandstone	Early Albian	5° 49' 30.758"	73° 41' 47.587"
CON–08–287	ANH–CON–08	CEOC	San Gil Sandstone	Early Albian	5° 57' 12.630"	73° 36' 31.512"
CON–08–1310	ANH–CON–08	CEOC	San Gil Sandstone	Early Albian	5° 57' 12.630"	73° 36' 31.512"
CON–08–1376	ANH–CON–08	CEOC	Paja	Barremian and Aptian	5° 57' 12.630"	73° 36' 31.512"
CON–08–2575	ANH–CON–08	CEOC	Paja	Barremian and Aptian	5° 57' 12.630"	73° 36' 31.512"
COS–05–261	ANH–COS–05	Villa de Leyva	Conejo	Turonian to Santonian	5° 31' 54.705"	73° 49' 49.929"
COS–05–1059	ANH–COS–05	Villa de Leyva	Conejo	Turonian to Santonian	5° 31' 54.705"	73° 49' 49.929"
COS–14–370	ANH–COS–14	Villa de Leyva	Villa de Leyva	Late Hauterivian	5° 35' 01.356"	73° 31' 30.586"
COS–14–650	ANH–COS–14	Villa de Leyva	Villa de Leyva	Late Hauterivian	5° 35' 01.356"	73° 31' 30.586"
COS–14–678	ANH–COS–14	Villa de Leyva	Ritoque	Late Valanginian – early Hauterivian	5° 35' 01.356"	73° 31' 30.586"
COS–14–1506	ANH–COS–14	Villa de Leyva	Ritoque	Late Valanginian – early Hauterivian	5° 35' 01.356"	73° 31' 30.586"
COS–15–893	ANH–COS–15	Villa de Leyva	San Gil Sandstone	Early Albian	5° 32' 37.037"	73° 38' 06.689"
COS–15–1323	ANH–COS–15	Villa de Leyva	San Gil Sandstone	Early Albian	5° 32' 37.037"	73° 38' 06.689"
COS–15–1330	ANH–COS–15	Villa de Leyva	Paja	Barremian and Aptian	5° 32' 37.037"	73° 38' 06.689"
COS–15–2220	ANH–COS–15	Villa de Leyva	Paja	Barremian and Aptian	5° 32' 37.037"	73° 38' 06.689"
INFA–4727	Infantas–1613	MMV	La Luna	Turonian to Santonian	6° 55' 38.423"	73° 46' 43.388"
INFA–6243	Infantas–1613	MMV	La Luna	Turonian to Santonian	6° 55' 38.423"	73° 46' 43.388"
INFA–6396	Infantas–1613	MMV	El Salto	Cenomanian	6° 55' 38.423"	73° 46' 43.388"
INFA–6472	Infantas–1613	MMV	El Salto	Cenomanian	6° 55' 38.423"	73° 46' 43.388"
INFA–6480	Infantas–1613	MMV	Simití	Middle and late Albian	6° 55' 38.423"	73° 46' 43.388"
INFA–8840	Infantas–1613	MMV	Simití	Middle and late Albian	6° 55' 38.423"	73° 46' 43.388"
INFA–8650	Infantas–1613	MMV	Tablazo	Early Albian	6° 55' 38.423"	73° 46' 43.388"
INFA–9358	Infantas–1613	MMV	Paja	Barremian and Aptian	6° 55' 38.423"	73° 46' 43.388"
INFA–9364	Infantas–1613	MMV	Paja	Barremian and Aptian	6° 55' 38.423"	73° 46' 43.388"
RIO–3496	Río de oro–14	Catatumbo	Mito Juan	Early Maastrichtian	9° 05' 37.499"	72° 54' 04.926"
RIO–4220	Río de oro–14	Catatumbo	Mito Juan	Early Maastrichtian	9° 05' 37.499"	72° 54' 04.926"
RIO–4780	Río de oro–14	Catatumbo	Colón (Lower)	Early Campanian	9° 05' 37.499"	72° 54' 04.926"
RIO–5392	Río de oro–14	Catatumbo	Colón (Lower)	Early Campanian	9° 05' 37.499"	72° 54' 04.926"
RIO–5768	Río de oro–14	Catatumbo	La Luna	Turonian to Santonian	9° 05' 37.499"	72° 54' 04.926"
RIO–5775	Río de oro–14	Catatumbo	La Luna	Turonian to Santonian	9° 05' 37.499"	72° 54' 04.926"
RIO–6259	Río de oro–14	Catatumbo	Capacho	Middle and late Albian	9° 05' 37.499"	72° 54' 04.926"
SAR–7336	Sardinata–n2	Catatumbo	La Luna	Turonian to Santonian	8° 30' 15.474"	72° 39' 04.879"
SAR–7460	Sardinata–n2	Catatumbo	La Luna	Turonian to Santonian	8° 30' 15.474"	72° 39' 04.879"

Table 3. Sandstone samples located outside of main sections.

Sample	Area	Formation	Age	Latitude N	Longitude W
GPS–89	Barichara	Tablazo	Early Albian	7° 10' 51.343"	73° 16' 47.387"
GPS–270	Aguachica	Aguachica	Late Aptian	8° 13' 01.122"	73° 31' 10.134"
GPS–500	Llanos Foothills	San Luis	Early Maastrichtian	4° 50' 00.469"	73° 12' 28.233"
GPS–501	Llanos Foothills	San Antonio	Early Campanian	4° 50' 11.561"	73° 12' 50.548"
GPS–502	Llanos Foothills	Chipaque	Turonian to Santonian	4° 50' 31.771"	73° 12' 59.524"
GPS–506	Llanos Foothills	Alto de Caqueza	Late Hauterivian	4° 51' 51.308"	73° 14' 02.402"
GPS–510	Llanos Foothills	Batá	Berriasian	4° 51' 42.523"	73° 16' 07.012"
GPS–511	Llanos Foothills	Farallones	Carboniferous	4° 52' 55.098"	73° 16' 15.635"
GPS–518	Llanos Foothills	Fómeque	Barremian and Aptian	5° 00' 14.466"	73° 30' 14.414"
GPS–520	Llanos Foothills	Une (Middle)	Middle and late Albian	5° 03' 09.896"	73° 31' 38.813"
GPS–526	Llanos Foothills	Une (Upper)	Cenomanian	5° 04' 52.142"	73° 37' 09.574"
GPS–540	Barichara	Tambor	Berriasian to Valanginian	6° 31' 31.234"	73° 02' 37.969"
GPS–541	Barichara	Tambor	Berriasian to Valanginian	6° 36' 23.379"	73° 02' 47.256"
GPS–543	Barichara	Rosablanca (Upper)	Late Hauterivian	6° 25' 11.723"	73° 09' 31.939"
GPS–549	Barichara	Tambor	Berriasian to Valanginian	6° 53' 59.656"	73° 20' 58.413"
GPS–551	Barichara	Tambor	Berriasian to Valanginian	6° 53' 54.205"	73° 21' 50.441"
GPS–553	Barichara	Tablazo	Early Albian	6° 56' 30.482"	73° 22' 40.936"
GPS–555	Barichara	Simití	Middle and late Albian	7° 08' 32.549"	73° 17' 56.712"
GPS–556	Aguachica	Aguachica	Late Aptian	8° 14' 00.073"	73° 31' 56.083"
GPS–564	Catatumbo	Aguardiente	Early Albian	7° 57' 38.309"	72° 49' 36.168"
GPS–568	Catatumbo	Guayacán	Cenomanian	7° 53' 32.915"	72° 42' 04.787"
GPS–571	Barichara	Tambor	Berriasian to Valanginian	6° 52' 00.669"	73° 03' 21.267"
GPS–572	Barichara	Tambor	Berriasian to Valanginian	6° 54' 57.911"	73° 01' 53.909"
GPS–579	Villeta	La Naveta	Late Hauterivian	4° 30' 23.637"	74° 34' 11.221"
GPS–599	Villeta	Socotá	Early Albian	5° 01' 03.675"	74° 31' 02.152"
GPS–602	Villeta	Útica	Late Hauterivian	5° 11' 14.769"	74° 27' 57.707"
GPS–619	Villeta	Murca	Berriasian to Hauterivian	5° 04' 07.443"	74° 26' 00.059"
GPS–1210	Villa de Leyva	San Gil Shale	Middle and late Albian	5° 34' 30.881"	73° 30' 19.854"
GPS–1211	Villa de Leyva	Villa de Leyva	Late Hauterivian	5° 35' 06.535"	73° 30' 52.170"
GPS–1220	Llanos Foothills	Macanal (Middle)	Early Valanginian	4° 45' 07.809"	73° 33' 38.372"
GPS–1238	Llanos Foothills	Une (Lower)	Early Albian	4° 25' 03.396"	73° 59' 13.992"
OU	CEOC	La Tabla	Early Maastrichtian	5° 41' 00.988"	74° 11' 15.624"

Other important ages present in both Paleozoic and Cretaceous strata (Figures 5–7; Table 4) are in the ranges of 450 to 650 Ma (Ediacaran to Ordovician) and 900 to 1100 Ma, which correspond with the late Mesoproterozoic to early Neoproterozoic Grenvillian Orogeny. Middle and early Mesoproterozoic particles around 1300 and 1500 Ma and a few Paleoproterozoic and Archean particles are also present, clearly indicating a cratonic source area to the E. There are no particles of Jurassic or Cretaceous age. The lower part of the Cretaceous section contains more abundant Paleozoic particles than the upper part because Proterozoic particles became dominant as the Paleozoic sedimentary basement was eroded. These results are similar to those reported from the E side of the Eastern Cordillera by Horton et al. (2010), who indicated that Paleozoic grains in the range of 500 to 400 Ma are more common in the lower part of the Cretaceous section, whereas Paleoproterozoic and Mesoproterozoic grains of 2000 to 950 Ma become dominant in the upper part.

4.1.2. Villeta area, CEOC, and MMV

Along the W margin of the basin, the source areas of the Cretaceous strata were quite different from those for the Llanos Foothills on the E basin margin. Mesoproterozoic and Paleozoic particles were also present in the Central Cordillera but in lower

Table 4. Detrital zircon U–Pb provenance ages (Ma).

Sample	Number of particules	Formation	Area	Youngest ages	Youngest ages group	Important age groups			Oldest ages group
GPS–500	108	San Luis	Llanos Foothills	477 ± 22	450–500	1000–1050	1550–1600	1750–1800	2500–2550
QSA–92	73	Aguacaliente	Llanos Foothills	462 ± 22	450–500	1000–1050	1200–1250	1450–1500	3900–3950
GPS–501	103	San Antonio	Llanos Foothills	548 ± 28	450–550	900–950	1300–1350	1650–1700	2000–2050
GPS–502	102	Chipaque	Llanos Foothills	435 ± 26	400–450	1000–1050	1150–1200	1450–1500	2500–2550
GPS–526	96	Une (Upper)	Llanos Foothills	410 ± 18	400–450	1000–1050	1300–1350	1800–1850	2100–2150
GPS–520	95	Une (Middle)	Llanos Foothills	463 ± 12	450–500	950–1000	1250–1300	1450–1500	2750–2800
GPS–1238	99	Une (Lower)	Llanos Foothills	304 ± 26	300–350	550–600	950–1000	1450–1500	2350–2400
GPS–518	79	Fómeque	Llanos Foothills	335 ± 12	300–350	600–650	900–950	1550–1600	1950–2000
GPS–506	108	Cáqueza Sandstone	Llanos Foothills	480 ± 54	450–500	950–1000	1150–1200	1450–1500	2600–2650
GPS–1220	105	Macanal	Llanos Foothills	282 ± 26	250–300	400–450	900–950	1400–1450	1900–1950
GPS–510	108	Batá	Llanos Foothills	312 ± 10	300–350	400–450	900–950	1050–1100	1750–1800
GPS–511	98	Farallones	Llanos Foothills	311 ± 12	300–350	500–550	1000–1050	1150–1200	3500–3550
CON6–1322	87	Churuvita	Villa de Leyva	445 ± 17	400–450	1000–1050	1450–1500	1800–1850	2200–2250
GPS–1210	99	San Gil Shale	Villa de Leyva	525 ± 24	500–550	1250–1300	1500–1550	2650–2700	2050–2100
CON8–1181	76	San Gil Sandstone	Villa de Leyva	332 ± 30	300–350	550–600	850–900	1350–1400	1800–1850
GPS–1211	83	Villa de Leyva	Villa de Leyva	428 ± 14	400–450	850–900	950–1000	1150–1200	1950–2000
COS14–1550	102	Arcabuco	Villa de Leyva	401 ± 12	400–450	900–950	950–1000	1450–1500	2650–2700
QAD–15	84	La Luna	Barichara	86 ± 5	50–100	200–250	1000–1100	1450–1500	2050–2100
QS–14.8	84	El Salto	Barichara	536 ± 30	500–550	1300–1350	1750–1800	1900–1950	2650–2700
GPS–555	83	Simití	Barichara	473 ± 25	450–500	950–1000	1500–1550	1750–1800	2000–2050
GPS–553	92	Tablazo	Barichara	401 ± 17	400–450	450–500	1500–1550	1750–1800	2600–2650
GPS–89	91	Tablazo	Barichara	361 ± 13	600–650	900–1000	1500–1550	1750–1800	2750–2800
GPS–543	103	Rosablanca	Barichara	269 ± 19	400–450	500–550	900–1000	1150–1200	2100–2150
GPS–540	109	Tambor	Barichara	373 ± 18	350–400	450–550	900–1000	1400–1450	2100–2150
GPS–541	94	Tambor	Barichara	139 ± 9	100–150	150–200	200–250	400–450	2000–2050
GPS–571	104	Tambor	Barichara	287 ± 13	350–400	500–550	950–1000	1400–1450	2050–2100
GPS–572	104	Tambor	Barichara	158 ± 8	150–200	200–250	400–450	950–1000	2000–2050
GPS–551	104	Tambor	Barichara	256 ± 11	250–300	400–450	1000–1050	1500–1550	1800–1850
GPS–549	100	Tambor	Barichara	145 ± 6	150–200	200–250	350–400	400–450	2100–2150
RR1–15	100	La Luna	Catatumbo	90 ± 4	50–100	100–150	150–200	1000–1050	1400–1450
GPS–568	99	Guayacán	Catatumbo	487 ± 77	450–600	1300–1350	1500–1550	1700–1750	3250–3300
RR–00	82	Capacho	Catatumbo	442 ± 18	400–450	1300–1350	1550–1600	1750–1800	2000–2050
GPS–564	106	Aguardiente	Catatumbo	420 ± 16	500–550	950–1000	1150–1200	1450 –1500	2100–2150
GPS–556	89	Aguachica	Aguachica (MMV)	145 ± 8	100–150	150–200	900–950	1000–1100	1700–1750
GPS–270	106	Aguachica	Aguachica (MMV)	164 ± 6	170–186	150–200	200–250	600–650	950–1000
OU	28	La Tabla	CEOC	78 ± 6	50–100	100–150	1200–1250	1550–1600	2100–2150
GPS–599	99	Socotá	Villeta	142 ± 10	100–150	150–200	950–1000	1150–1200	2500–2550
GPS–602	102	Útica	Villeta	138 ± 7	100–150	150–200	250–300	1150–1200	3000–3050
GPS–579	64	La Naveta	Villeta	128 ± 13	100–150	150–200	200–250	950–1000	1200–1250
GPS–619	98	Murca	Villeta	135 ± 6	100–150	150–200	250–300	950–1000	2850–2900

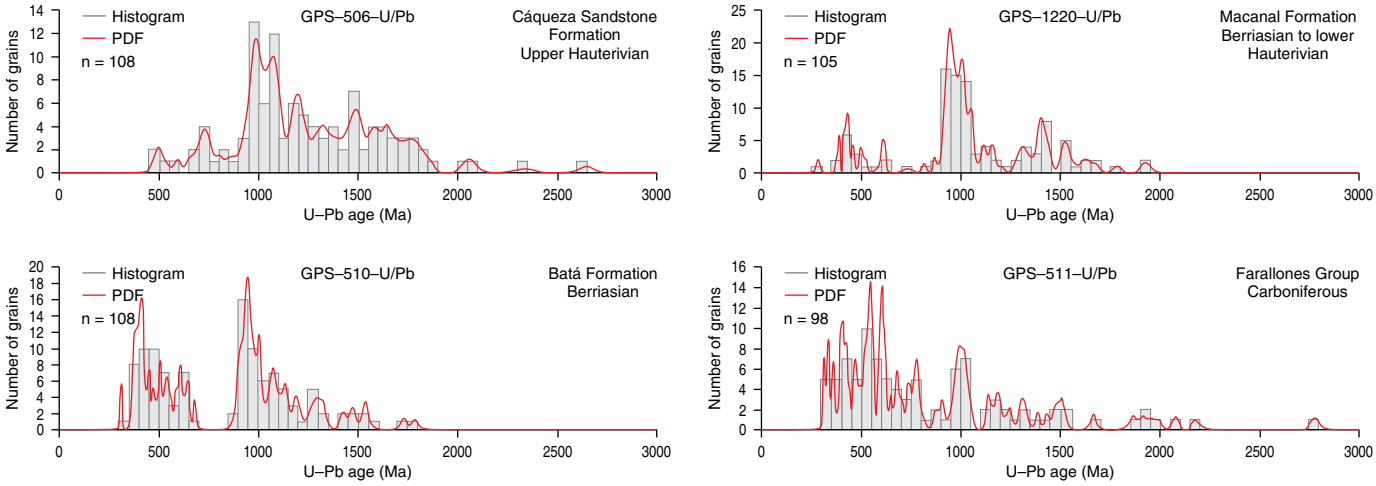

Figure 5. Detrital zircon U–Pb ages from the Paleozoic sedimentary basement and Berriasian to Hauterivian units from the E foothills of the Eastern Cordillera.

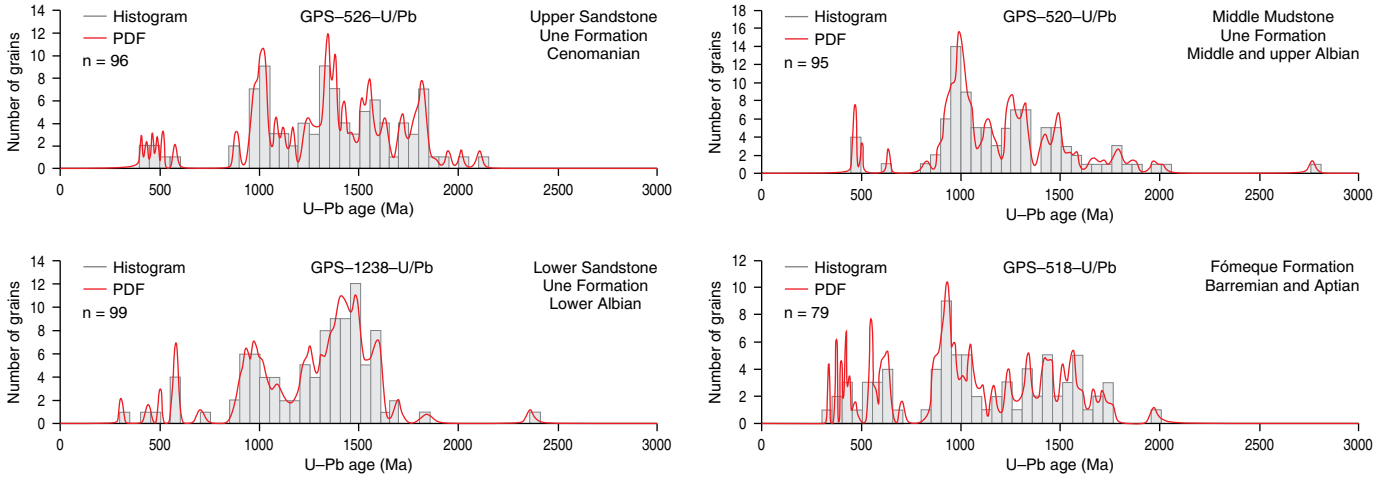

Figure 6. Detrital zircon U–Pb ages of Barremian to Cenomanian units from the E foothills of the Eastern Cordillera.

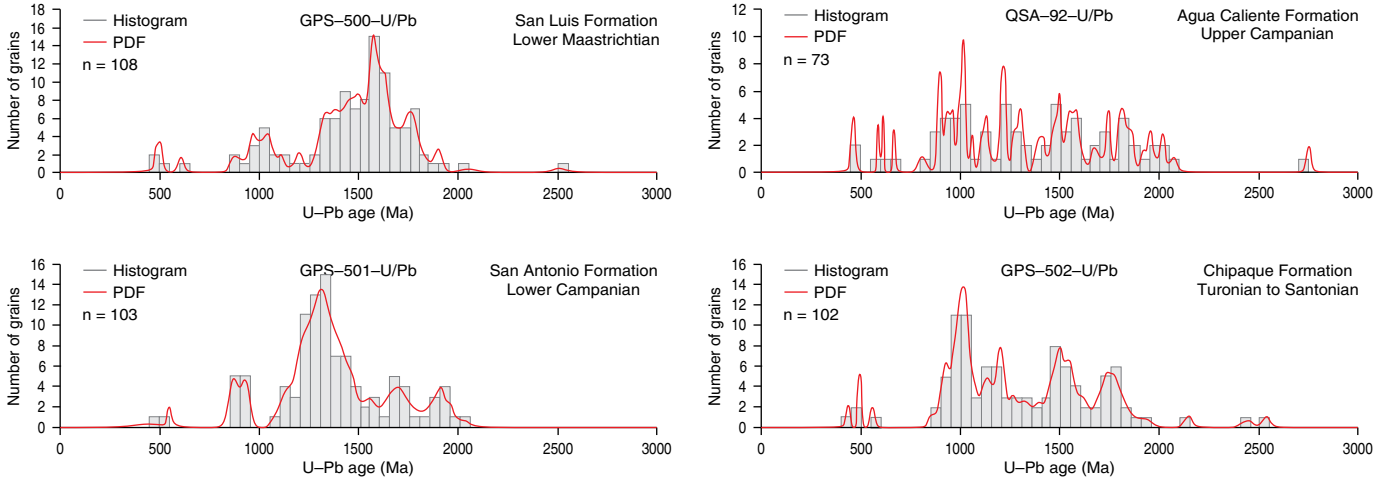

Figure 7. Detrital zircon U–Pb ages of Turonian to lower Maastrichtian units from the E foothills of the Eastern Cordillera.

proportions than in the E sources. The age of zircon particles (Figures 8, 9; Table 4) is dominated by Lower Cretaceous rocks derived from magmatic and volcanic activity in the Central Cordillera and by abundant Jurassic rocks exhumed before and during the development of the Cretaceous basin. Sample GPS–619 from the Murca Formation contains 27 particles that cluster at 135 ± 6 Ma, which is within the Berriasian to Hauterivian biostratigraphic age range of the unit. The highest frequency includes 37 particles in the 150 to 200 Ma Jurassic age range. Sample GPS–579 from La Naveta Formation contains 11 particles concentrated at 128 ± 13 Ma and 35 particles (highest frequency) in the 150 to 200 Ma Jurassic age range. The Útica Formation (GPS–602) contains 12 grains focused at 138 ± 7 Ma and the highest frequency (35 grains) in the 150 to 200 Ma Jurassic age range. The upper sandstone/conglomerate members of the Murca, La Naveta, and Útica Formations are contemporaneous regressive units of late Hauterivian age, which include shoreface and fluvial deposits sourced from the Central Cordillera magmatic arc. The names have been inconsistently used to include upper Hauterivian regressive conglomerates and sandstones of fluvial and shoreface origin and Berriasian to lower Hauterivian mudstones with minor sandstone interbeds of marine origin. The ages of zircon grains presented here are consistent with the Berriasian to Hauterivian biostratigraphic range of the units. The sedimentary petrography and the grain size paleogeography of the sandstones (Guerrero, 2002a; Moreno, 1990, 1991) also indicate provenance from the Central Cordillera.

The lower Albian sandstones of the Socotá Formation show the same pattern of Jurassic to Early Cretaceous grains. Sample GPS–599 includes 5 particles centered at 142 ± 10 Ma and 12 particles in the 150 to 200 Ma Jurassic age interval. Interestingly, it also includes a number of Proterozoic dates at approximately 1150 ± 29 Ma, which could be interpreted as derived from the Guiana Shield, but Jurassic and Cretaceous sources are not represented there, so the source area should not have been the shield. The unit was deposited in a regressive shoreface dominated by storms, with sediments sourced from rivers draining the Central Cordillera.

The lower Maastrichtian La Tabla Formation from the CEOC (sample OU) contains 3 zircon grains at 78 ± 6 Ma (Campanian) and 139 ± 5 Ma (Berriasian to Valanginian), along with 2–4 grains around 1200 Ma and 1500 to 1900 Ma (Figure 9).

The western provenance of zircon particles from the Central Cordillera is also observed for samples from the Magdalena Valley. The basal sandstones in the Aguachica area, which are outside the central rift of the basin, are of late Aptian age. Older Cretaceous strata of Berriasian to early Aptian age from the main rift of the basin (present–day Eastern Cordillera) are nonexistent in the Aguachica area. The stratigraphy is similar to that exposed in the Upper Magdalena Valley (UMV), where the oldest Cretaceous strata of the Yaví Formation and the Lower and Middle Members of the Caballos Formation are of Aptian age (Guerrero, 2002b; Guerrero et al., 2000). These Aptian units also rest unconformably on Jurassic igneous and volcaniclastic rocks: the Saldaña Formation in the UMV and the Noreán Formation in the northern sector of the MMV. The oldest ammonites collected from the marine beds transitionally overlying the conglomerates and sandstones of the Aguachica section are of late Aptian age, so that the section is definitely younger than the succession from the western foothills of the Eastern Cordillera near Bucaramanga. The Aguachica section was deposited on the W side of the basin, unlike the Barichara–Bucaramanga section, which was supplied from the E side of the basin. Consequently, the Tambor, Rosablanca, Paja, and Tablazo Formations are not present. A different stratigraphic nomenclature should be used for those areas of the Magdalena Valley west of the Early Cretaceous border faults. We propose the name Aguachica Formation for the transgressive upward–fining fluvial succession of conglomerates, sandstones, and red mudstones of Aptian age, which rest unconformably on the Noreán Formation and are overlain transitionally by marine strata of late Aptian to Maastrichtian age. The Aguachica Formation name is applied only to the fluvial strata; the overlying marine beds should receive formal names different from those of rocks in the Barichara–Bucaramanga.

The youngest zircon grains from the Aguachica Formation (Figure 9; Table 4) at the base of the Cretaceous section near Aguachica in the Cesar Department (GPS–556) are in the range of 145 ± 8 Ma; the highest age frequency of the sample (70 grains) is in the Jurassic interval from 150–200 Ma. Of these, 37 grains are clustered at 174 ± 8 Ma. A few grains with Triassic and older ages are also present.

Sample GPS–270 contains 102 grains in the 150–200 Jurassic interval; of these, 84 grains are within the age of 178 ± 8 Ma. The youngest grain has an age of 164 ± 6 Ma, and only 4 grains are older than Jurassic.

The provenance ages of the basal Cretaceous section from the MMV coincide with the ages reported by Horton et al. (2015) from the Cocuyo, Guane, and Cagui wells. They recognized peaks at 170 to 185 Ma for the coarse–grained nonmarine section (Aguachica Formation) and 175 to 190 Ma for the finer–grained marine deposits.

Proterozoic U–Pb ages have been reported from several localities on the E flank of the Central Cordillera; for instance, Villagómez et al. (2011) reported zircon crystals from La Miel Orthogneiss with ages of 1700 to 450 Ma and a major peak at approximately 1200 Ma. They also reported zircon crystals from a quartzite in the Cajamarca Complex with a peak age of approximately 240 Ma and 500 to 600 Ma and 1000 to 1200 Ma populations. Ordóñez–Carmona et al. (2006) reported Sm/Nd TDM ages of approximately 1710 and 1790 Ma from El Vapor Gneiss, which also has a metamorphic Rb/Sr age of 894 ± 36 Ma. The Tierradentro amphibolite has a K/Ar age of 1360 ± 270 Ma (Vesga & Barrero, 1978). El Hígado Amphibolite has an Ar/Ar age

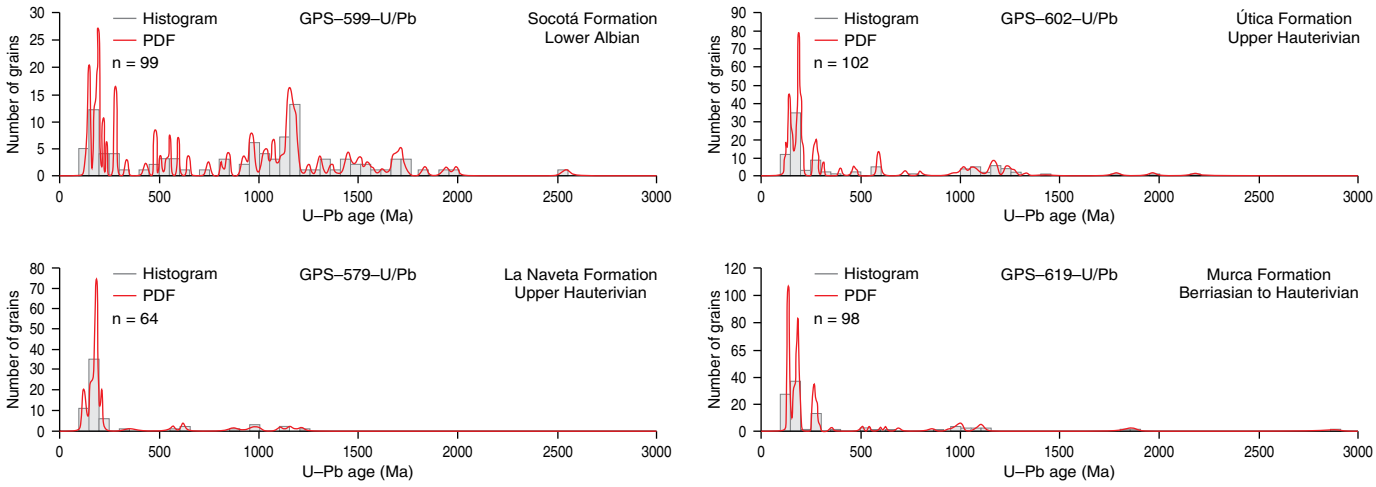

Figure 8. Detrital zircon U–Pb ages of Berriasian to lower Albian units from the Villeta Area.

of 911 ± 2 Ma (Restrepo–Pace et al., 1997). Granulites from the San Lucas Gneiss yield a U–Pb age of 1124 ± 22 Ma and a Sm/Nd TDM age of 1600 Ma, as reported by Clavijo et al. (2008).

It is evident that Proterozoic ages are not exclusive to eastern sources in the Guiana Shield but are also present in western sources today along the E flank of the Central Cordillera, which was the uplifted magmatic/metamorphic arc and constituted the western margin of the Cretaceous Colombian back–arc basin. The Central Cordillera as the source of Proterozoic particles was also indicated by Horton et al. (2015), but they concluded that the Cretaceous strata at the MMV were supplied from both E and W sources, including the Central Cordillera serranía de San Lucas, the Eastern Cordillera Santander Massif, and the Guiana Shield.

We postulate that although the Proterozoic particles could have been derived either from the Guiana Shield or from the Central Cordillera, there is certainly a notable difference in the frequency of the Proterozoic particles, which are far more abundant when the source area is the Guiana Shield. However, what is markedly different and unique in the western source area (Central Cordillera) is the presence of Jurassic and Cretaceous particles, which are not present to the E in the Guiana Shield. Therefore, we prefer to interpret our data from the Villeta and MMV areas as indicating a single source area in the Central Cordillera.

The possibility of units derived from both the E and W flanks of the basin would only be conceivable for a trunk fluvial system along the basin axis during the early rifting (Berriasian to Valanginian) stage, as discussed below for the Tambor Formation. However, the units studied are shoreface marine sandstones with younger ages that could not possibly be sourced from both sides of the basin because the E and W shorefaces of the basin had already been separated since the late Valanginian by the deeper offshore muds and marls in the center of the basin. It is impossible for particles to cross from one side of the basin to the deepest axis of the seaway and subsequently reach the opposite shoreface. Eastern Cordillera sources in exposed horsts are impossible because the present–day massifs (Santander, Floresta, and Quetame) were already covered by marine strata during the late Valanginian. The crystalline basement of those massifs was covered by Lower Cretaceous to middle Miocene strata and was only exposed again during the late Miocene to the present due to uplift of the Eastern Cordillera. Since late Valanginian times, the only possible sources for the Cretaceous back–arc basin were the Guiana Shield and the Central Cordillera, supplying the opposite E and W shorelines.

4.1.3. Villa de Leyva Area

The central portions of the Eastern Cordillera repeat the pattern from the SE of the basin in the Bogotá–Villavicencio–San Luis area and show provenance from the Guiana Shield.

Samples from the ANH stratigraphic wells CON and COS were collected, along with outcrop samples, from the proximities of Villa de Leyva in Boyacá Department. The samples processed include the Arcabuco, Villa de Leyva, Paja, San Gil Inferior Sandstone, and Churuvita Formations (Figure 10; Table 4). The Villa de Leyva area is dominated by zircon particles of Paleozoic, Proterozoic, and Neoarchean ages, from 300 to 2700 Ma. There are neither Jurassic nor Cretaceous particles. The samples include peaks at 1000 Ma, 1500 Ma, and 1700 Ma, related to rocks from the late Mesoproterozoic to early Neoproterozoic Grenvillian Orogeny, and particles from the late Paleoproterozoic to early Mesoproterozoic Río Negro–Juruena Province.

4.1.4. Barichara Area

Cretaceous samples from Santander Department (Figures 11–13) were collected on both flanks of Los Cobardes Anticline and on both margins of the Sogamoso River valley near the type section of the units. The Cretaceous succession, which begins with a cobble to pebble conglomerate included in the

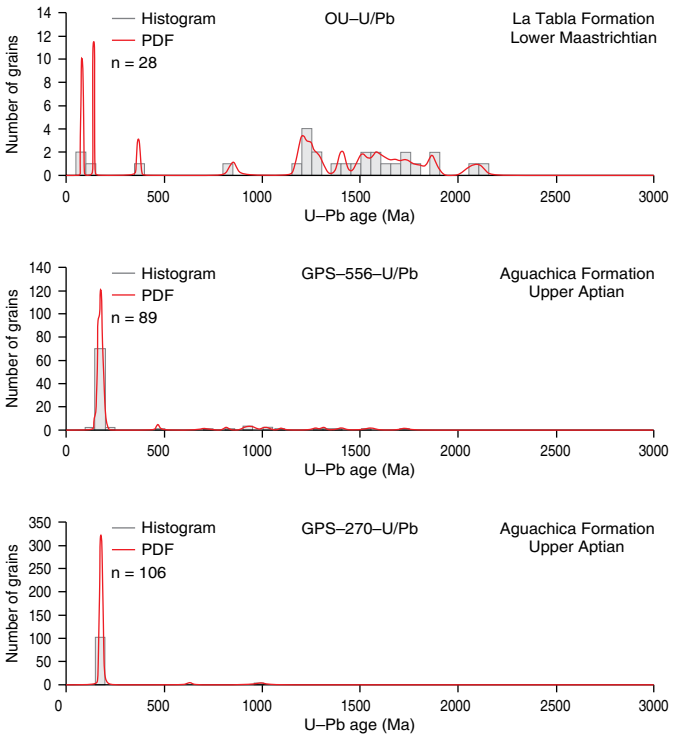

Figure 9. Detrital zircon U–Pb ages of units from the CEOC (Otanche) and MMV (Aguachica).

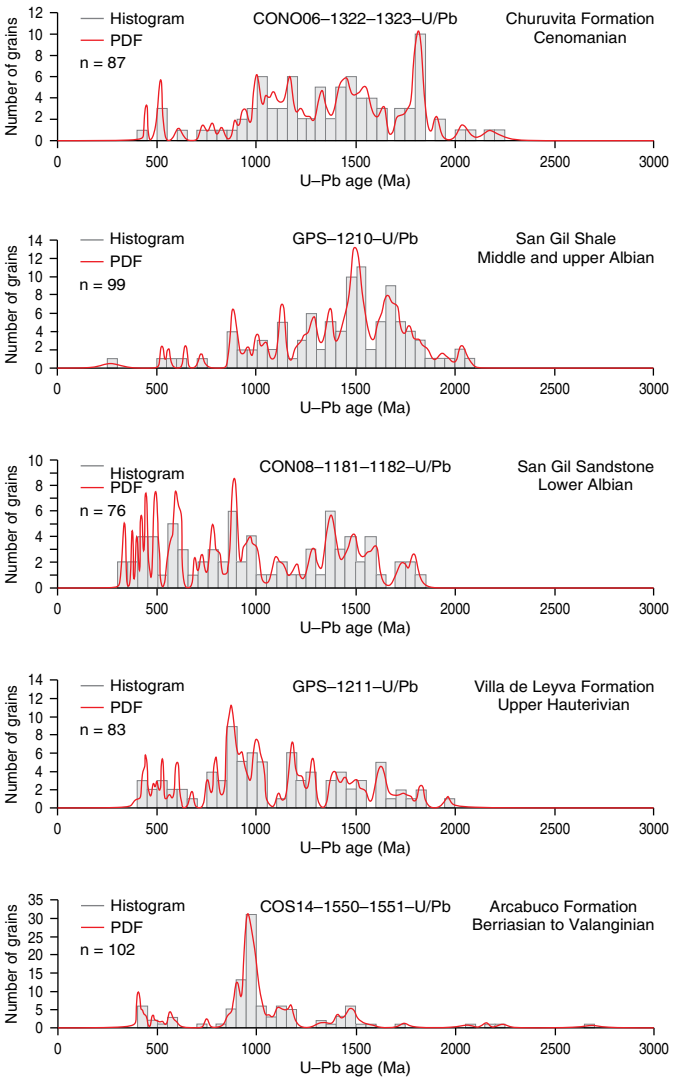

Figure 10. Detrital zircon U–Pb ages of Berriasian to Cenomanian units from the Villa de Leyva area.

fluvial strata of the lower part of the Tambor Formation, rests unconformably on older igneous, metamorphic, and sedimentary units. Prior to the back–arc subsidence that originated the Cretaceous basin, older units were faulted and exhumed through the Late Jurassic Andean orogeny. During early rift development of the Cretaceous back–arc system, rivers from both the E and W sides of the basin fed a trunk river that drained northward toward the Caribbean.

Samples GPS–549 and GPS–551 collected along the road from Zapatoca to San Vicente indicate both a source from the Central Cordillera and a source from the Guiana Shield (Figure 11). The sample with the lower stratigraphic position (GPS–549) was derived from the Central Cordillera because it contains 23 Jurassic grains from 150 to 200 Ma and 9 Triassic grains from 200 to 250 Ma. The youngest particle has an age of 145 ± 6 Ma in the Tithonian to Berriasian time span. An Early Jurassic age peak is placed at 190 ± 9 Ma, and an Early Devonian peak is placed at 410 ± 12 Ma, which are the main age populations of the sample. The stratigraphically higher sample (GPS–551) contains Proterozoic particles with 1000 to 1500 Ma age peaks along with a few Paleozoic but no Jurassic particles, suggesting derivation from the Guiana Shield.

Samples GPS–571 and 5 GPS-572 were collected from Mesa de Los Santos, which exhibits a good reference section of the Tambor Formation. Sample GPS–571 contains Proterozoic and Paleozoic age peaks but no Jurassic grains, consistent with derivation from the Guiana Shield. Sample GPS–572 has a mixture of Jurassic, Paleozoic, and Proterozoic ages, so it was sourced from the Central Cordillera. The particle with the youngest age is Late Jurassic (158 ± 8 Ma). In total, 13 Triassic and Jurassic particles are present, with a peak at approximately 196 ± 6 Ma. The highest frequency, with a total of 21 grains, occurs in the range of 400 to 450 Ma (Silurian and Early Devonian).

Samples GPS–540 and GPS–541 were collected from a monocline structure near Curití, on the San Gil to Mogotes road, from strata of the Tambor Formation resting unconformably over the early Paleozoic Silgará Schist and Mogotes Batholith. The sample (GPS–540) was sourced from the Guiana Shield; it contains Proterozoic particles, mainly 900 to 1000 Ma, and early Paleozoic particles but no Jurassic or Cretaceous particles (Figure 12). The Curití sample (GPS–541) was sourced from the Central Cordillera and contains 3 Early Cretaceous grains with a central age of 139 ± 9 Ma, consistent

with the Berriasian to Valanginian age range of the unit. The highest frequency (33 grains) is in the Triassic to Jurassic age interval, with a peak at 202 ± 13 Ma.

The Tambor Formation is transitionally covered by offshore marine strata of the lower part of the Rosablanca Formation, which includes marlstones and biomicrites deposited during late Valanginian to early Hauterivian progressive flooding of the basin. The shoreline and the rivers definitely migrated to the W because the overlying units contain particles derived only from the Guiana Shield. Sample GPS–543 from the upper Hauterivian regressive shoreface sandstones and sandy biosparites of the upper part of the Rosablanca Formation includes Proterozoic grains in the 900–1000 Ma age interval (highest frequency), along with a few Paleozoic grains with a youngest age of 269 ± 19 Ma (Figure 12; Table 4). Since there are no Mesozoic particles, we conclude that the unit was sourced from the Guiana Shield.

During the Barremian and Aptian, the basin was again extensively flooded, reaching farther to the E and W and also to the S, covering a larger area of Colombia and parts of Venezuela and Ecuador. Shale and marlstone beds (Fómeque, Paja, and Yuruma Formations) reach thicknesses of 600 m in the basin center. Basal conglomerates and sandstones were deposited along the basin margins in the present–day Magdalena Valley (Yaví and Aguachica Formations) and Llanos Foothills. Strata overlying the Paja Formation, including the Tablazo, Simití, and El Salto Formations, contain particles derived from the Guiana Shield.

Sample GPS–89 of the lower Albian Tablazo Formation contains age populations of approximately 400–450 Ma, 900–1000 Ma, and 1500–1550 Ma; the youngest particle is 361 ± 13 Ma (Figure 12; Table 4). Sample GPS–553 from the same unit has age populations of 450–500 Ma, 1500–1550 Ma, and 1750–1800 Ma; the youngest particle is 401 ± 17 Ma (Figure 13).

Sample GPS–555 from a very fine sandstone within the middle and upper Albian Simití shale has age peaks of approximately 450–500 Ma, 950–1000 Ma, 1500–1550 Ma, and 1750–1800 Ma (Figure 13; Table 4). The youngest particle has an age of 473 ± 25 Ma. The ages from El Salto Formation have peak populations at 1750–1800 Ma and 1900–1950 Ma, with a youngest age of 536 ± 30 Ma. None of the samples from the Tablazo, Simití, and El Salto Formations contain Mesozoic particles, so these units were sourced from the Guiana Shield.

Sample QAD–15 from the upper part of La Luna Formation is a pale gray bentonite claystone that contains 69 zircon particles with a central age of 86 ± 5 Ma (Figure 13; Table 4), which we interpret as volcanic ash falls transported by wind from the Central Cordillera magmatic arc during a time close to the Coniacian/Santonian boundary. The sample also includes a few Proterozoic particles (12 in total) that we believe were derived from the Guiana Shield, as well as other Albian and Cenomanian samples. We postulate that the Late Cretaceous zircon particles from La Luna Formation were not transported by rivers draining the Central Cordillera because of the absence of Jurassic particles, which are a unique mark of this source area.

The rocks of La Luna Formation from the QAD section include mainly biomicrites of foraminifera, transformed into diagenetic cherts with 50 to 70 % quartz and 20 to 45 % calcite plus dolomite. Minor storm beds of phosphatic bio–pelmicrites are also present with fluorapatite contents up to 60% and P_2O_5 contents up to 18%. The illite contents range from 3 to 5 %, with an exceptional value of approximately 16%, so the terrigenous contribution was generally very low, except for the wind–transported volcanic ash beds, which were dispersed on both sides of the basin. The U–Pb dating of distal volcanic ash zircons transported by wind has also been reported from the Cretaceous of Australia by Barham et al. (2016) and from the Miocene of North America by Smith et al. (2018).

4.1.5. Catatumbo Area

Finally, the areas south of Cúcuta exhibit a high frequency of Proterozoic particles derived from the Guiana Shield. Important peaks present in the Aguardiente, Capacho, and Guayacán Formations are approximately 1000 Ma, 1500 Ma, and 1800 Ma (Figure 14; Table 4). An exception is a volcanic tuff sample (RR1–15) that comes from the lower part of La Luna Formation at Riecito River and contains a high frequency of particles (94 zircon grains) with an age of 90 ± 4 Ma, near the Turonian/Coniacian time boundary. These particles are interpreted as wind–transported volcanic ash. The terrigenous content of La Luna Formation biomicrites is generally very low, so there are very few zircon particles (only 6) of older ages, which could have been transported by fluvial streams and storm currents to lower offshore depths.

ICP–OES analyses of the foraminiferal biomicrites from Riecito River reveal very low aluminum (Al_2O_3) contents less than 1%, with 46 to 55 % calcium (CaO) and 40 to 43 % volatile components, (mostly CO_2) loss on ignition (LOI), indicating 86 to 98 % calcite contents. The partially silicified biomicrites contain 42 to 49 % SiO_2, 2 to 4 % Al_2O_3, and 43 to 50 % calcite. The terrigenous clay and silt contents are very low except in the wind–transported volcanic ash beds present in the unit.

4.2. XRD, Heavy Minerals, and ICP–MS/OES Analyses

XRD mineral analyses, heavy mineral analyses, ICP–OES, and ICP–MS elemental analyses (Tables 5–9) from several localities and stratigraphic positions also help in the identification of the source areas for the basin.

Diagenesis during sediment burial modifies the crystallinity of clay minerals, but there is no documented evidence of metamorphism or clay neomorphism in the strata, so the clay mineralogy depends mostly on the rock types from the source areas

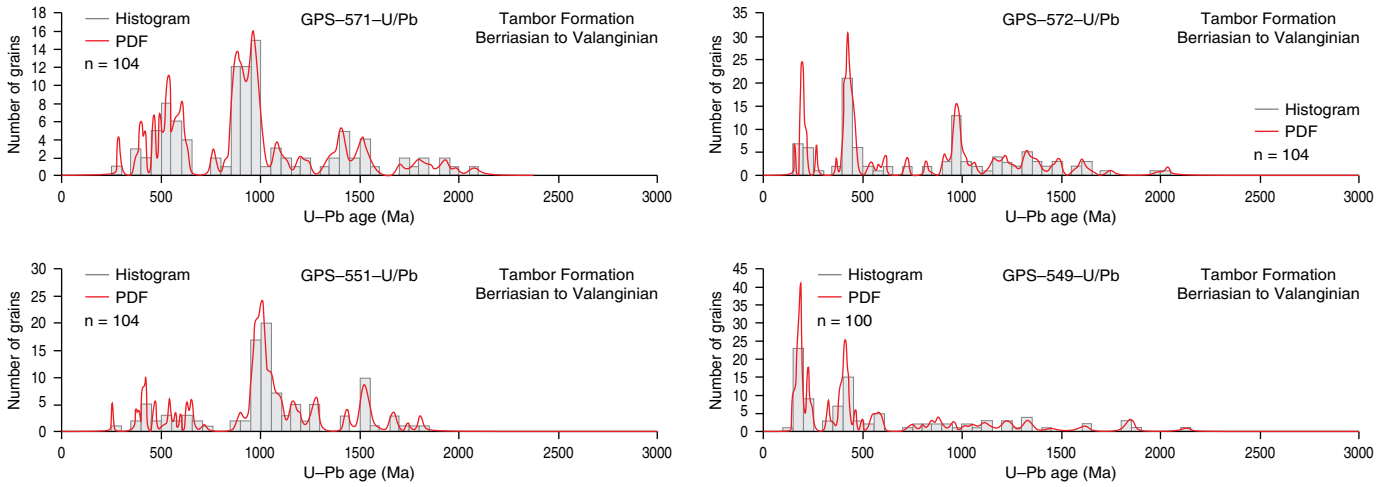

Figure 11. Detrital zircon U–Pb ages of the Tambor Formation from the Barichara area.

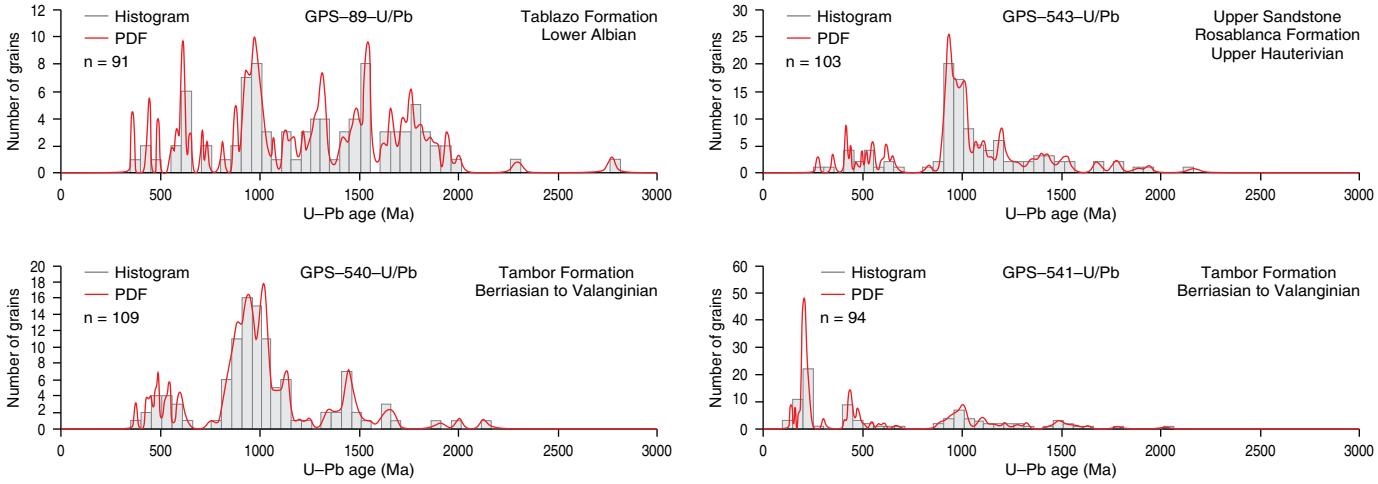

Figure 12. Detrital zircon U–Pb ages of Berriasian to lower Albian units from the Barichara area.

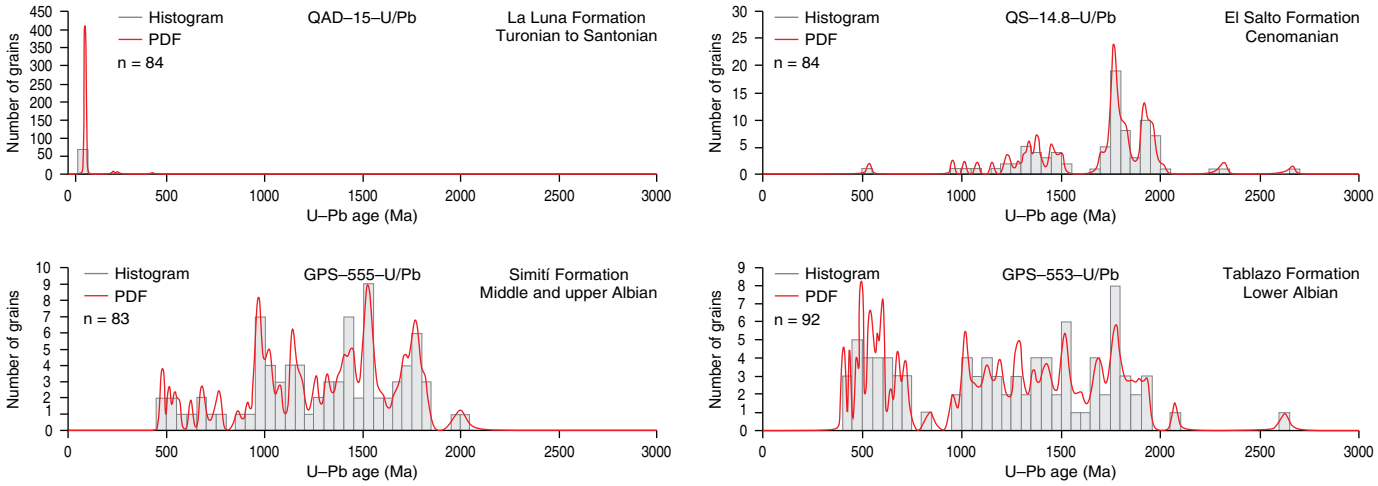

Figure 13. Detrital zircon U–Pb ages of lower Albian to Santonian units from the Barichara area.

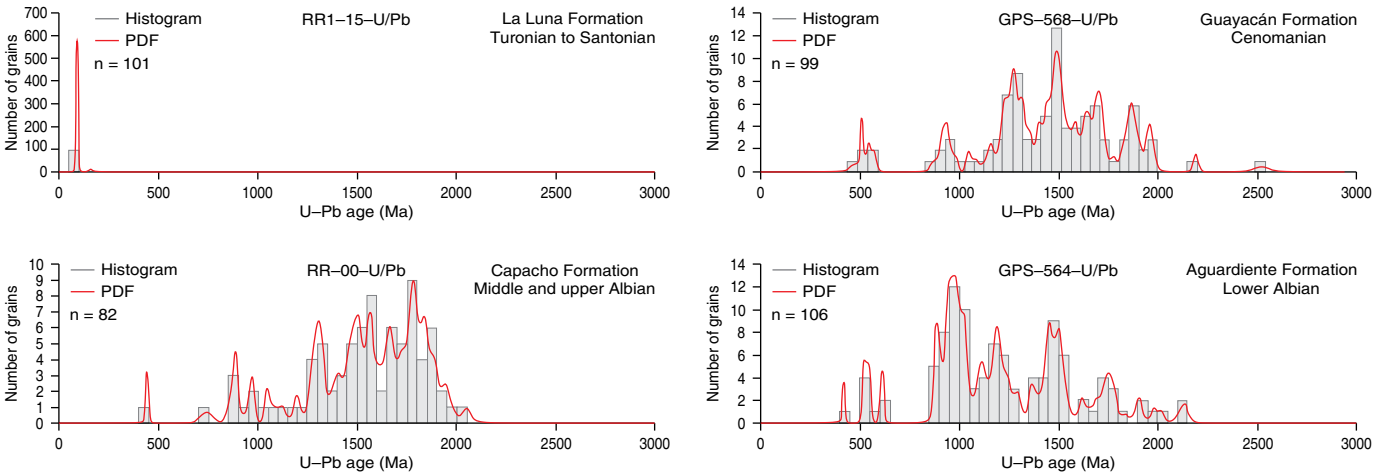

Figure 14. Detrital zircon U–Pb ages of lower Albian to Santonian units from the Catatumbo area.

of the basin. For instance, Bonilla et al. (2011) documented low degrees of kaolinite and illite crystallinity for Maastrichtian strata of the Upper Guadalupe Group and lower part of the Guaduas Formation, indicating slight diagenesis. For illite, they reported a Kubler crystallinity index of approximately 0.9 to 1.1, which would indicate a temperature of approximately 100 °C and correspond to burial diagenesis at approximately 3 km, which also matches the approximate 3 km thickness of the overlying Paleogene section. Considering an average geothermal gradient of 25 °C/km and the thickness of the underlying Campanian to Berriasian strata of approximately 4 km, the temperature of the basal strata from the Cretaceous section was approximately 200 °C, still within the diagenetic zone. Because of these observations, we consider that the clay mineralogy primarily reflects the nature of the rocks from the provenance areas. The clay mineralogy of source areas from the Guiana Shield should reflect the weathering of granites and recycled Paleozoic strata. The clay mineralogy of source areas from the Central Cordillera should reflect the weathering of continental igneous and metamorphic rocks, along with accreted oceanic basalt and gabbro.

The XRD analyses presented here show that clay minerals are common in shale units with source areas on the eastern side of the basin but are also present along the western side. The highest average percentages of kaolinite (Al_2O_3 $2SiO_2$ $2H_2O$) of approximately 50 to 55 % (Figure 15; Table 5) are from the Paja Formation in its type section (QLP) and the Une and Chipaque Formations along the San Antonio Creek (QSAU and QSAC). These shale intervals include lower average percentages of quartz silt (18 to 28 %) and illite (7 to 18 %). The high percentages of kaolinite would indicate several cycles of weathering in the tropical rainforest of the Guiana Shield.

The highest average percentages of illite in the range of 60 to 65 % (Figure 16; Table 5) are from shales of the Simití and El Salto Formations in the Infantas (INFA) 1613 well and from the Hilo Formation in the Otanche section (O); both are located toward the W side of the basin. These shale units contain lower average percentages of quartz silt (37 to 38 %) and no kaolinite. Since illite includes K, Mg, and Fe in the structure, high values of these elements are also found in the ICP–OES analyses of Otanche samples, approximately 9% Fe_2O_3 and 6% K_2O, which are among the highest values of these elements in the basin. The highest K_2O content in the study (6.4%) is from a sample (O–85) of the Otanche section.

Chlorite is present in minor amounts compared to kaolinite and illite. The highest average percentage of chlorite (22%) from XRD analyses comes from the shales in the lower part of the Murca Formation at the Tobia River section (RT) in the Villeta area. These samples include an average of 34% quartz silt particles, with lesser amounts of illite (11%), calcite (10%), kaolinite (8%), and dolomite (7%). Chlorite is most likely derived from low–grade metamorphic rocks sourced from the Central Cordillera.

Montmorillonite is present in very minor amounts in sections from the SE side of the basin, usually associated with kaolinite. The highest average percentages of montmorillonite (3 to 5 %) come from the Chipaque and Aguacaliente Formations at the San Antonio Creek sections.

The total ICP–OES distribution of aluminum (expressed as Al_2O_3) is highest in the central sector of the basin and in the Llanos Foothills (Figure 17; Table 6). It is coincident with the distribution of kaolinite and illite, which are the most abundant clay minerals. The highest Al_2O_3 individual values (26 to 30 %) are from the central and SE areas of the basin in wells COS–15, CON–7, CON–8, CON–6, and COS–5, La Paja Creek in Santander (QLP), and the Llanos Foothills along San Antonio Creek (QSAU and QSAC).

There are several important elements associated with the clay content of black shales from the basin, which also help to discriminate between western and eastern sources. The highest contents of titanium (1.7% TiO_2), zirconium (1337 ppm),

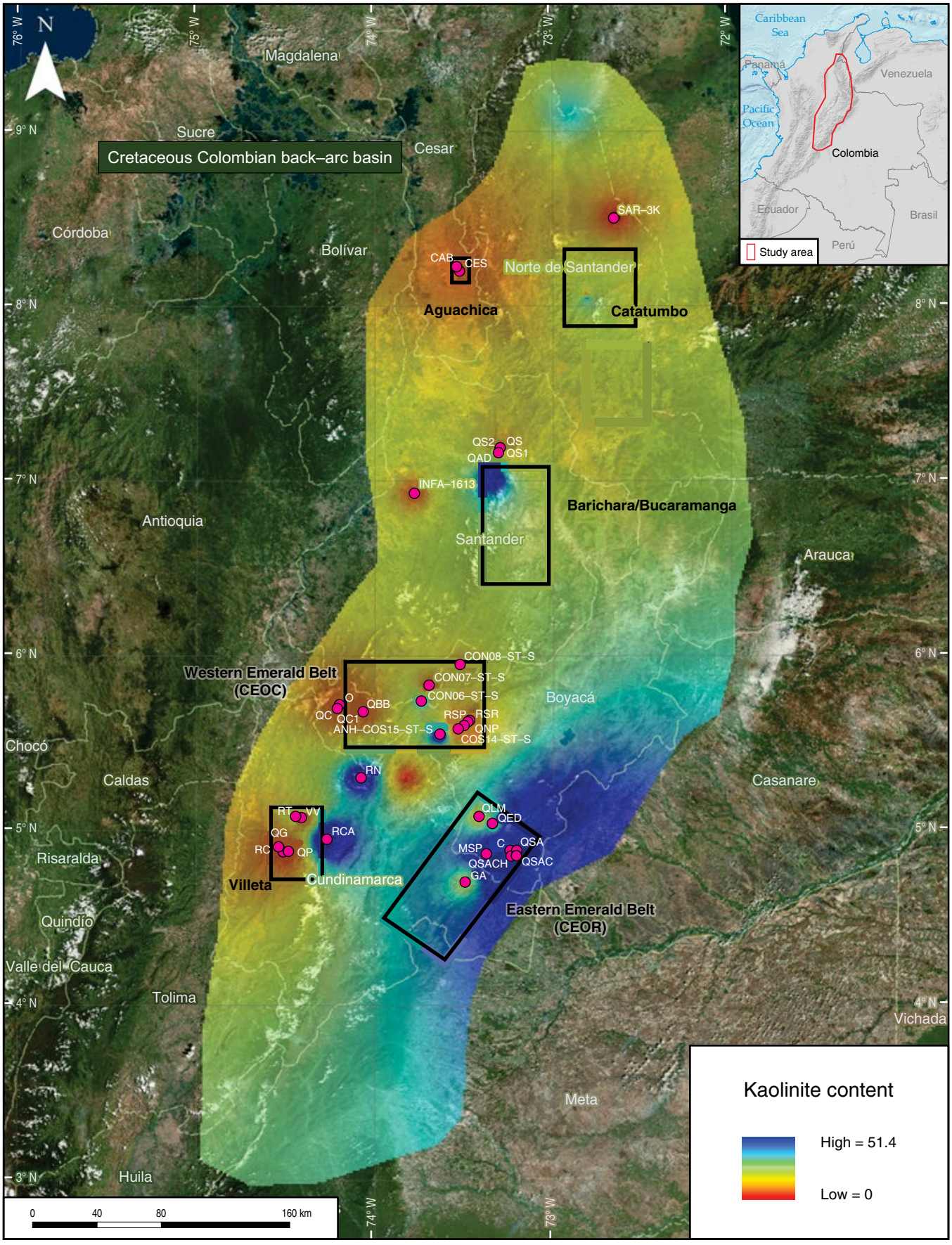

Figure 15. Kaolinite contents from XRD. Values plotted are average percentages per locality.

Table 5. XRD mineralogy (average percentage per section).

Section	Area	Formation	Quartz	Dolomite	Illite/Muscovite	Pyrophyllite	Kaolinite	Calcite	Chlorite	Pyrite	Rutile	Koenenite	Siderite	Gypsum	Ankerite	Albite	Anatase	Montmorillonite	Fluorapatite	Total phyllosilicates
QSAC	Llanos Foothills	Chipaque	27.5		11.1		54.1				2.0							3.8		69.0
QSAU	Llanos Foothills	Une	26.7		6.5		52.3					0.6	13.3				0.6			58.8
QLP	Barichara	Paja	17.5		17.5		50.0	1.4		4.6		1.7					7.3			67.5
QSACH	Llanos Foothills	Chipaque	55.6		9.1		28.9		0.4	0.8							0.4	4.8		43.2
QSA	Llanos Foothills	Aguacaliente	50.6		9.7		26.7		2.1	1.5	1.2		1.8					2.8		41.3
RN	Villeta	Pacho	37.6	0.4	6.4	8.3	23.2	9.1	7.5	4.7	0.6	0.2		0.6	0.3		1.2			45.4
COS–15	Villa de Leyva	Paja	18.6		26.8	18.4	17.3			5.8	2.1	3.7	0.5	2.0	2.4					62.5
C	CEOR	Macanal	39.4		31.5		12.2			0.5	0.2	0.4	15.8							43.7
QED	CEOR	Fómeque	28.9	2.1	9.5	11.3	10.4	24.8	3.3	0.7	0.5				0.9	4.5	0.6			34.5
CON–7	Villa de Leyva	San Gil Shale	38.8	0.5	15.0	13.2	10.3	2.3	5.1	2.7	0.4	1.5	1.6		5.0		0.3			43.6
COS–5	Villa de Leyva	Conejo	58.0	5.5	5.7	5.8	8.8	7.8		2.4	0.5	1.4	1.2		2.9					20.3
CON–6	Villa de Leyva	Churuvita	64.0		15.5		7.8	2.4	3.2	0.9		0.9	2.6	0.3	1.8		0.3			26.5
CON–8	Villa de Leyva	Paja	22.5	2.3	11.8	27.4	7.7	14.8	0.1	3.2	0.3	2.8	1.8	2.6	2.4					47.0
CAB	Aguachica	La Luna	59.5		1.8	0.3	1.7	31.3	0.3	2.3			0.3						2.5	4.1
QS2	Barichara	La Luna	23.0		0.6		0.5	70.6		1.2			0.2		1.3				2.6	1.1
QAD	Barichara	La Luna	50.1	4.8	4.5		0.5	30.1		1.5		0.5							8.0	5.0
SAR–3K	Catatumbo	La Luna	26.7	1.6	3.7			61.3		1.4	0.7	0.4		1.0					3.2	3.7
RT	Villeta	Murca	33.7	6.5	11.2		7.7	9.7	21.9	2.3	1.0	1.9		0.2	3.9					40.8
QP	Villeta	Hilo	46.4	1.8	14.5		0.4	26.5	3.7	3.6		1.5		1.2	0.2					18.6
QC	UMV	Lidita Inferior	59.3		26.9		3.0	0.7	8.8			0.7	0.4				0.2			38.7
GA	CEOR	Macanal	33.2		35.2		7.4	4.6	8.6	4.7	0.7			5.6						51.2
MSP	CEOR	Macanal	28.9		35.2			0.2			1.6					33.6				35.2
RSP	Villa de Leyva	Villa de Leyva	27.9		35.8	16.5	2.2		7.0	4.3	2.1	4.2								61.5
COS–14	Villa de Leyva	Ritoque	40.2	2.9	38.0		2.1	3.0	7.1	2.4	1.6	0.6		0.1	2.0					47.2
QBB	CEOC	Furatena	49.4		39.6		1.4		9.6											50.6
QNP	Villa de Leyva	Paja	29.2	11.1	42.2	0.8		4.8	4.1	1.6				0.4	5.8					47.1
O	CEOC	Hilo	38.4		59.7					0.8		1.1								59.7
INFA–1613	MMV	Simití	37.0	0.5	62.5															62.5
INFA–1613	MMV	El Salto	37.1		62.9															62.9

thorium (52 ppm), niobium (46 ppm), hafnium (36 ppm), and tantalum (4 ppm) in the study come from a shale sample (COS15–2054) of the Paja Formation in the Villa de Leyva area (Tables 6–8). As indicated before, the unit was sourced from the eastern side of the basin, which has more differentiated continental crust than the western sources.

In contrast, the highest contents of chromium (0.105% Cr_2O_3), copper (825 ppm), molybdenum (372 ppm), arsenic (121 ppm), antimony (94 ppm), selenium (79 ppm), thallium (13 ppm), and silver (9 ppm) in the study come from the shales of the Hilo Formation in the Otanche section (O–05, 15, 25, 40, 45, and 75), which also have very high illite contents. The unit was sourced from the western side of the basin, which included the magmatic/metamorphic arc and accreted oceanic crust.

The light REE of the cerium group have the maximum values (Figure 18; Table 9) of the study in a siltstone sample (COS14–1575) from the upper part of the Arcabuco Formation, in the ANH COS–14 well, in the vicinity of Villa de Leyva: Ce (619

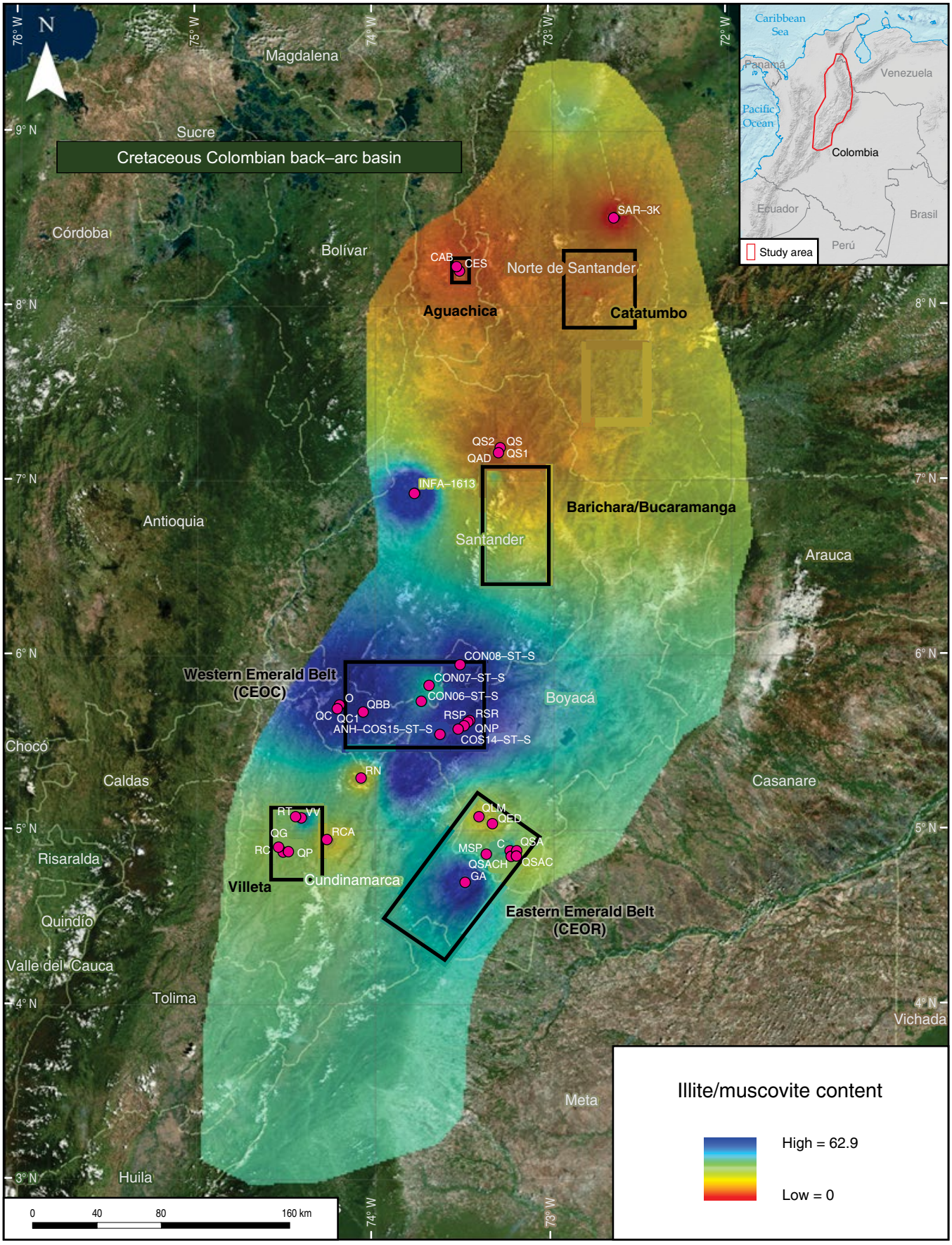

Figure 16. Illite/muscovite contents from XRD. Values are average percentages per locality.

ppm), Nd (315 ppm), La (276 ppm), Pr (82 ppm), Sm (50 ppm), and Eu (8 ppm). In contrast, the heavy REE of the yttrium group have the maximum values of the study in a sample (RT–10) from the lower part of the Murca Formation in the Tobia River section: Y (231 ppm), Dy (40 ppm), Gd (27 ppm), Er (19), Yb (11 ppm), Ho (8 ppm), Tb (6 ppm), and Tm (2 ppm). The high contents of the yttrium group would indicate an ultramafic source in accreted oceanic crust situated along the western flank of the basin, while the cerium group indicates more differentiated continental crust on the eastern flank of the basin.

Another important mineral that indicates provenance is apatite, which shows higher percentages (Figure 19) in the western part of the basin and is related to igneous and metamorphic sources in the Central Cordillera. Samples with heavy mineral analyses containing high percentages of terrigenous apatite come from the Murca, Trincheras, Socotá, Hilo, and Pacho Formations from the western side of the Eastern Cordillera.

An important part of the reported apatite is related to phosphatic biomicrites and has an authigenic origin because of biological accumulation in fish. The highest percentages of fluorapatite from XRD analyses are from La Luna Formation in the Aguadulce Creek (8%) and La Sorda Creek (3%) near Bucaramanga, the Sardinata 3K well near Cúcuta (3%), and Caño Agua Blanca near Aguachica (3%). The highest contents of P_2O_5 from ICP–OES analyses (Table 7) are from La Luna Formation at La Leche Creek near Cúcuta (26%) and Aguadulce Creek (18%).

The distribution of apatite in La Luna Formation is related to the distributions of quartz and calcite (Figures 20, 21; Tables 5–7) because the unit consists mostly of biomicrites composed of planktonic foraminifera and fish remains (containing authigenic fluorapatite), along with diagenetic cherts. Since the unit was deposited during the Turonian to Santonian transgressive and highstand sea levels, the terrigenous clay input was very low or completely absent, and the rocks consist of microfossil particles deposited offshore. Textures include wackestone and packstone beds; the latter could originate from high productivity but are usually the result of repetitive storm events that concentrate the available particles. Quartz enters the system much later during diagenesis, replacing calcite. The foraminifera and the calcareous mud matrix are partially to totally replaced by quartz, and the rock becomes a diagenetic chert, as illustrated for the Lidita Inferior and Lidita Superior Formations of the UMV (Guerrero et al., 2000). The quartz is obtained from the terrigenous units above and below the original calcareous strata. These terrigenous units are in turn partially replaced by calcite mobilized from the limestones in a two–way exchange of calcite and quartz during diagenesis. All cherts from the basin are diagenetic, including those of the Hilo, Lomagorda, La Luna, La Frontera, Lidita Inferior, and Lidita Superior Formations. Radiolaria and diatoms are almost completely absent, so no oceanic cherts are present.

The highest calcium (CaO) contents of the study (40 to 55 %), obtained from ICP–OES analyses (Table 7), come from biomicrite limestones of La Luna Formation in the N part of the basin (Catatumbo, Aguachica, and Barichara areas). These samples have CO_2 loss on ignition (LOI) of 33 to 43 %, except for those with higher phosphate content (3 to 26 % P_2O_5) or are partially replaced by diagenetic quartz (1 to 19 % SiO_2). The content of Al_2O_3 is less than 3% because of the nearly complete absence of clay minerals; the content of Fe, Mg, Na, and K is usually less than 1%. Samples from the same sections that are extensively replaced by quartz to create diagenetic cherts have increased SiO_2 contents (49 to 66 %) and decreasing percentages of CaO (12 to 22 %) and LOI (16 to 22 %).

The highest contents of SiO_2 (59 to 79 %) in diagenetic cherts (Table 7) are from La Luna Formation (Barichara, Aguachica, and MMV), Lidita Inferior and Lidita Superior Formations (UMV), Hilo Formation (Villeta), and La Frontera Member of the Conejo Formation (Villa de Leyva).

Associated with the phosphates biologically concentrated by fish in the biomicrites and cherts of La Luna Formation (Tables 7, 8) are the highest contents of uranium (27 to 89 ppm), nickel (231 to 468 ppm), and strontium (1521 to 2506 ppm) in the study. The SAR–7443 sample from the Catatumbo area contains the highest values of uranium and nickel. The highest values of vanadium in the study (1901 to 3865 ppm) are present in cherts and biomicrites of the Hilo Formation (QP from the Villeta area) and La Luna Formation (QLL, RR1, and QS2 from the Catatumbo and Barichara areas).

4.3. Elements Related to Gabbro–Diorite–Tonalite Intrusions and Valanginian to Cenomanian Hydrothermal Activity During the Synrift Stage

The highest contents of scandium come from the southeastern side of the basin in the sections at Vereda Cachipay (29 ppm) and the San Pedro emerald mine (24 ppm). In these areas, the anomalous content of scandium in the Berriasian to lower Hauterivian shales of the Macanal Formation (Tables 6, 8) does not seem to be related to the source areas of sediment; instead, it would be related to hydrothermal activity linked to the Early Cretaceous intrusion of several gabbro, diorite, and tonalite bodies documented by Vásquez et al. (2005, 2010). Scandium was originally present in the structure of pyroxenes and amphiboles of the gabbroic bodies because of its affinity with minerals in mafic melts. The XRD analyses of the rocks related to the San Pedro emerald mine reveal a very anomalous 34% albite content, which is also the highest percentage in the study. The highest contents of sodium (2 to 7 % Na_2O) in the basin come from the San Pedro emerald mine area because of the high content of hydrothermal albite ($NaAlSi_3O_8$). The

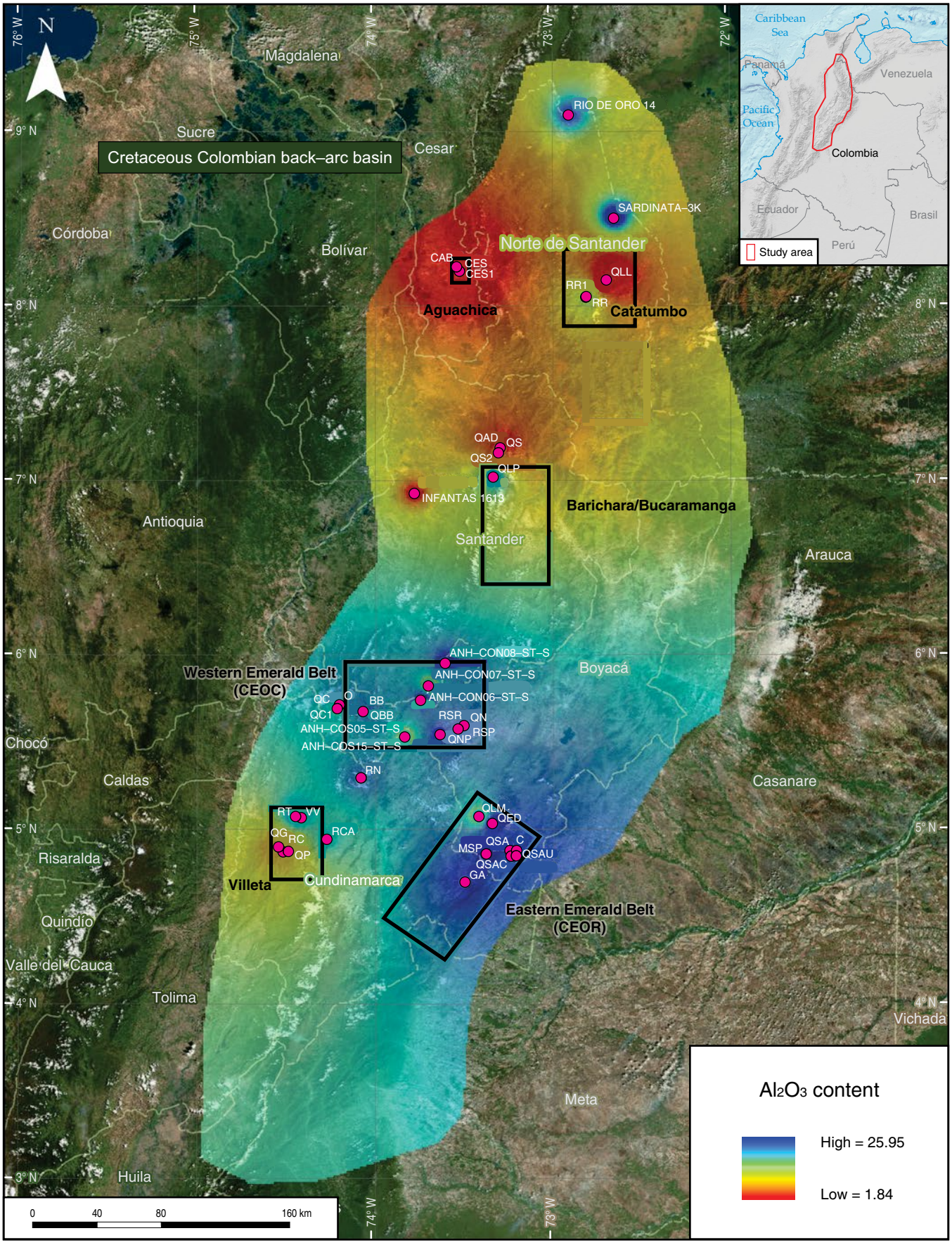

Figure 17. Aluminum distribution from ICP–OES analyses. Values are average percentages per locality.

Table 6. Major elements percentages (shale/siltstone samples).

Sample	Area	Formation	SiO_2	Al_2O_3	Fe_2O_3	MgO	CaO	Na_2O	K_2O	TiO_2	P_2O_5	MnO	Cr_2O_3	Ni	Sc	LOI	Total
COS15–1553	Villa de Leyva	Paja	50.76	29.95	4.49	0.47	0.60	0.89	2.95	0.96	0.18	0.01	0.015	40	19	8.5	99.78
CON7–1125	Villa de Leyva	San Gil Shale	47.54	29.18	6.45	1.03	0.34	0.56	2.30	0.91	0.12	0.02	0.015	45	20	11.3	99.77
CON8–1796	Villa de Leyva	Paja	46.58	28.16	4.25	0.67	2.26	0.68	2.82	0.82	0.17	0.01	0.018	52	18	13.3	99.74
QSAU–18	Llanos Foothills	Une	47.99	27.32	6.22	0.97	0.28	0.04	2.88	1.03	0.10	0.08	0.012	39	19	12.9	99.82
QLP–35	Barichara	Paja	46.41	26.42	4.36	0.62	2.57	0.19	1.92	0.80	0.14	0.01	0.021	66	18	16.2	99.66
QSAC–40	Llanos Foothills	Chipaque	47.69	26.35	7.04	1.12	0.60	0.23	1.95	0.99	0.11	0.05	0.026	24	19	13.7	99.86
CON6–1405	Villa de Leyva	Churuvita	50.05	25.82	6.82	1.06	0.54	0.26	2.95	1.04	0.18	0.04	0.012	35	19	11.0	99.77
COS5–269	Villa de Leyva	Conejo	50.86	25.65	4.50	0.77	0.48	0.59	2.06	0.87	0.12	<0.01	0.016	24	16	13.9	99.82
RSP–30	Villa de Leyva	Villa de Leyva	50.53	25.46	6.80	0.99	0.32	0.83	3.53	1.06	0.22	0.02	0.021	69	21	10.0	99.78
QED–30	CEOR	Fómeque	51.84	25.11	4.89	1.18	2.18	0.62	3.60	1.23	0.15	0.05	0.016	<20	21	8.9	99.77
O–85	CEOC	Hilo	57.18	25.06	1.05	1.13	0.02	0.13	6.43	0.78	0.13	<0.01	0.023	<20	21	7.7	99.63
QED–35	CEOR	Fómeque	51.93	24.98	6.53	1.04	0.24	0.60	3.34	1.28	0.17	<0.01	0.016	22	22	9.6	99.73
RN–60	Villeta	Pacho	52.08	24.89	6.24	1.17	1.91	0.42	2.25	0.91	0.17	0.01	0.017	43	17	9.7	99.77
C–40	CEOR	Macanal	55.40	24.09	3.25	0.98	0.29	0.46	4.41	1.07	0.12	0.03	0.015	41	17	9.7	99.82
COS14–522	Villa de Leyva	Villa de Leyva	51.97	23.98	6.10	1.15	1.17	0.92	4.12	0.89	0.15	0.02	0.017	66	20	9.3	99.79
O–55	CEOC	Hilo	48.10	23.82	5.04	1.00	0.03	0.17	5.15	0.65	0.14	<0.01	0.066	35	16	15.4	99.57
QNP–05	Villa de Leyva	Paja	47.40	23.77	6.01	1.22	4.26	0.58	3.27	0.93	0.16	0.07	0.025	92	18	12.1	99.80
QBB–00	CEOC	Furatena	55.10	23.71	3.89	1.11	0.35	1.30	3.51	0.87	0.16	<0.01	0.019	85	20	9.6	99.62
RT–15	Villeta	Murca	53.61	22.46	6.06	1.52	1.95	1.41	2.30	0.76	0.11	0.02	0.010	43	16	9.6	99.81
O–75	CEOC	Hilo	59.16	22.20	1.00	1.02	0.02	0.18	6.03	1.00	0.05	<0.01	0.105	<20	12	8.8	99.57
MSP–25	CEOR	Macanal	63.22	21.99	1.26	0.83	0.08	0.93	5.78	1.25	0.03	<0.01	0.016	<20	24	4.4	99.79
QSACH–25	Llanos Foothills	Chipaque	55.63	21.82	4.45	1.25	0.65	0.21	2.06	0.78	0.04	<0.01	0.025	24	15	12.9	99.82
COS14–1575	Villa de Leyva	Arcabuco	57.78	21.29	5.78	0.92	0.47	0.20	5.92	1.05	0.18	0.09	0.015	56	21	5.9	99.60
INFA–7359	MMV	Simití	55.83	21.18	5.60	1.20	0.45	0.50	1.55	0.84	0.23	0.02	0.015	36	15	12.4	99.82
GA–10	CEOR	Macanal	55.20	21.18	6.09	1.28	2.22	0.69	3.72	0.90	0.10	0.03	0.014	80	17	8.4	99.82
QSA–40	Llanos Foothills	Aguacaliente	54.09	19.84	5.98	1.83	1.30	0.19	2.08	0.69	0.20	0.03	0.028	<20	13	13.5	99.76
QP–20	Villeta	Hilo	54.15	19.53	3.37	0.84	5.12	0.33	1.49	0.58	0.29	0.01	0.018	143	15	13.8	99.53
GA–60	CEOR	Macanal	59.23	19.47	7.03	1.59	0.98	0.58	3.30	0.96	0.08	0.02	0.015	56	17	6.5	99.76
RT–10	Villeta	Murca	50.14	18.78	5.39	1.61	7.65	1.10	1.90	0.65	0.16	0.04	0.009	38	14	12.4	99.83
MSP–15	CEOR	Macanal	65.97	17.54	3.26	0.24	0.15	6.89	1.47	1.11	0.12	<0.01	0.014	<20	13	3.1	99.86
COS15–2054	Villa de Leyva	Paja	58.69	16.39	6.91	0.56	1.36	0.90	1.96	1.66	0.18	0.01	0.016	39	14	10.9	99.54
C–12	CEOR	Macanal	34.94	10.72	27.54	2.30	1.21	0.20	1.56	0.62	0.19	0.37	0.009	<20	29	20.2	99.86

shales of the Macanal Formation from the Gachalá section (GA) have the maximum contents of beryllium (6 to 9 ppm) in the basin. A younger unit from the same area that has a high content of albite (4.5%) according to the XRD analyses is the Barremian and Aptian Fómeque Formation from El Dátil Creek section (QED), which also has relatively high scandium (18 to 21 ppm) and beryllium (2 to 4 ppm) contents. The scandium and beryllium anomalies would be better explained by the Early Cretaceous hydrothermal activity that formed the emerald ($Be_3Al_2(SiO_3)_6$) mineralization.

The highest scandium values are restricted to Early Cretaceous sections that present some hydrothermal influence with calcite veins and intense micro fracturing. In addition to the Cachipay section (C) near Santa María de Bata (29 ppm), the San Pedro emerald mine (24 ppm), and El Dátil (22 ppm) from the Macanal and Fómeque Formations, high scandium values (20 to 23 ppm) are present in other units at other localities. Good examples are the Arcabuco and Villa de Leyva Formations from well COS–14 near Simijaca, the Villa de Leyva Formation (21 ppm) from the Samacá River section near Villa de Leyva, the Paja Formation (20 ppm) from well COS–15 near Ráquira, and the San Gil Superior Shales from well CON–7 near Puente Nacional. Relatively high scandium values are also present in the Berriasian to Hauterivian lower part of the Murca Formation

Table 7. Major elements percentages (biomicrite and chert samples).

Sample	Area	Formation	SiO_2	Al_2O_3	Fe_2O_3	MgO	CaO	Na_2O	K_2O	TiO_2	P_2O_5	MnO	Cr_2O_3	Ni	Sc	LOI	Total
SAR–7459	Catatumbo	La Luna	0.83	0.07	0.05	0.69	54.93	0.02	0.01	<0.01	0.10	<0.01	0.002	<20	<1	43.2	99.90
RR1–20	Catatumbo	La Luna	1.45	0.06	<0.04	0.36	54.79	<0.01	<0.01	<0.01	0.02	<0.01	<0.002	<20	<1	43.2	99.88
QLL–00	Catatumbo	La Luna	2.58	0.47	0.14	0.30	53.39	0.05	0.06	0.02	0.08	<0.01	<0.002	21	<1	42.8	99.89
CES1–00	Aguachica	La Luna	1.81	0.39	0.32	0.61	53.35	0.01	0.04	0.02	0.32	<0.01	0.005	24	<1	43.0	99.88
QLL–55	Catatumbo	La Luna	8.95	0.81	0.46	0.16	49.54	0.21	0.10	0.03	25.63	<0.01	0.021	45	5	13.4	99.31
QS2–35	Barichara	La Luna	10.93	0.58	0.23	0.49	47.92	0.01	0.08	0.03	0.13	<0.01	0.004	36	<1	39.4	99.80
QAD–65	Barichara	La Luna	15.17	1.32	0.35	0.17	44.47	0.07	0.15	0.05	18.32	<0.01	0.020	41	6	19.6	99.69
CAB–40	Aguachica	La Luna	12.8	2.56	0.71	0.43	44.45	0.04	0.41	0.10	3.37	0.02	0.017	37	4	34.9	99.81
CES1–10	Aguachica	La Luna	12.45	2.61	0.50	0.47	42.03	0.03	0.33	0.11	0.63	<0.01	0.017	63	3	40.4	99.58
SAR–7443	Catatumbo	La Luna	19.49	0.91	0.59	0.34	41.18	0.07	0.15	0.04	3.26	<0.01	0.019	468	2	33.0	99.05
QS2–50	Barichara	La Luna	18.24	1.78	0.44	0.40	39.77	0.06	0.27	0.07	0.42	<0.01	0.016	291	2	37.7	99.17
QP–270	Villeta	Hilo	21.42	2.53	2.54	0.48	39.24	0.02	0.21	0.08	0.15	0.05	0.009	126	5	33.0	99.73
CES–25	Aguachica	La Luna	19.28	3.37	0.92	0.42	38.19	0.07	0.41	0.14	0.48	<0.01	0.014	263	3	36.0	99.29
SAR–7410	Catatumbo	La Luna	21.10	2.91	0.95	0.59	37.53	0.32	0.49	0.08	0.77	<0.01	0.016	183	3	34.6	99.36
QS2–45	Barichara	La Luna	22.21	2.48	0.71	0.42	35.87	0.06	0.35	0.10	0.37	<0.01	0.019	357	2	34.8	97.39
CES–70	Aguachica	La Luna	28.05	1.65	0.46	0.29	34.79	0.04	0.22	0.06	0.38	<0.01	0.013	63	2	33.7	99.65
QLM–24	CEOR	Fómeque	29.54	4.45	2.36	0.61	33.24	0.12	0.48	0.33	0.10	0.06	0.003	<20	4	28.5	99.79
QAD–70	Barichara	La Luna	30.77	3.97	1.14	0.38	31.98	0.06	0.56	0.16	4.18	<0.01	0.021	108	4	26.5	99.72
QLP–10	Barichara	Paja	7.30	3.78	9.50	7.19	31.6	0.06	0.28	0.13	0.14	0.07	0.012	49	3	39.6	99.66
SAR–7379	Catatumbo	La Luna	34.37	3.04	0.93	0.45	29.92	0.39	0.54	0.11	0.73	<0.01	0.040	231	4	29.0	99.52
QAD–50	Barichara	La Luna	42.08	3.84	0.93	0.25	24.54	0.07	0.47	0.13	9.92	<0.01	0.021	75	7	16.4	98.65
QLL–10	Catatumbo	La Luna	44.03	2.85	0.91	0.42	23.89	0.19	0.38	0.07	0.31	<0.01	0.017	172	2	26.3	99.37
QLL–15	Catatumbo	La Luna	46.07	4.49	1.42	0.49	21.58	0.28	0.62	0.12	1.14	<0.01	0.028	227	3	22.9	99.14
RR1–35	Catatumbo	La Luna	48.71	4.00	1.22	0.34	21.57	0.05	0.46	0.11	1.23	<0.01	0.029	130	4	21.6	99.32
QG–257	UMV	Lidita Superior	59.43	3.33	1.21	1.42	16.20	0.24	0.40	0.12	0.35	<0.01	0.013	38	3	17.1	99.81
QAD–25	Barichara	La Luna	65.74	1.30	0.26	0.17	15.29	0.04	0.13	0.04	0.17	<0.01	0.018	87	<1	16.7	99.86
QP–445	Villeta	Hilo	57.62	4.57	1.03	0.28	14.82	0.02	0.47	0.20	0.23	0.01	0.027	187	5	19.9	99.18
CAB–115	Aguachica	La Luna	65.93	3.94	0.93	0.28	11.72	0.08	0.61	0.16	0.28	0.07	0.022	87	3	15.6	99.62
INFA–4724	MMV	La Luna	73.19	2.17	0.35	0.21	11.07	0.15	0.26	0.07	0.12	<0.01	0.010	53	2	12.2	99.80
COS5–985	Villa de Leyva	La Frontera	72.11	3.85	0.51	0.13	10.05	0.07	0.35	0.06	0.28	<0.01	0.011	70	2	12.3	99.72
QG–00	UMV	Lidita Inferior	78.91	4.55	1.20	0.42	5.49	0.26	0.61	0.18	0.39	<0.01	0.013	42	5	7.9	99.92

(14 to 16 ppm) at the Tobia River section (RT) and the lower part of the Furatena Formation (16 to 20 ppm) at Buriburi Creek (QBB) in the western part of the basin. The samples from QBB also have relatively high (2 to 4 ppm) beryllium contents. The presence of scandium in fluid inclusions in emeralds was also reported by Mantilla et al. (2008).

On the southwestern side of the basin, a vanadium anomaly (Table 8) is present in the shales from the upper part of the Hilo Formation at the Otanche section (O), near the emerald mines. The highest vanadium contents in the basin (2523 to 3865 ppm) come from the shales, marls, biomicrites, and diagenetic cherts of the middle and upper Albian Hilo Formation at the Piñal Creek (QP) and Otanche sections. The presence of vanadium was reported from emeralds of the CEOC by Pignatelli et al. (2015) in Valanginian to Hauterivian black shales and marlstones, assigned here to the Furatena Formation.

Other associated minerals in the shales include ankerite ($Ca(Fe,Mg,Mn)(CO_3)_2$) and dolomite ($CaMg(CO_3)_2$). According to XRD analyses (Table 5), the highest percentages are present in the Paja Formation shales (QNP) from the Villa de Leyva area, which contain 11.1% dolomite and 5.8% ankerite. The

Table 8. Minor elements in ppm (biomicrite and shale).

Sample	Area	Formation	Sc	Ba	Be	Hf	Nb	Rb	Sr	Th	U	V	Zr	Mo	Cu	As	Sb	Ag	Tl	Se
QLL–15	Catatumbo	La Luna	3	178	1	0.8	3.1	28.6	835.1	4.7	25.4	2404	26.9	97.4	73.9	28.5	9.2	1.0	0.8	10.4
QS2–45	Barichara	La Luna	2	136	<1	0.5	2.1	19.2	1394.2	2.5	20.5	2225	25.1	209.0	73.6	39.1	13.7	1.2	0.7	15.1
RR1–35	Catatumbo	La Luna	4	135	1	0.7	2.4	22.9	768.8	3.8	23.9	2125	30.8	63.1	88.5	50.2	9.9	0.7	0.7	8.5
QLL–10	Catatumbo	La Luna	2	282	1	0.4	1.9	16.1	683.6	2.7	12.7	1901	17.1	79.1	62.1	14.8	5.9	0.6	<0.1	16.7
CES–25	Aguachica	La Luna	3	865	<1	1.1	2.5	21.9	1510.8	2.7	24.4	1578	33.7	114.7	39.2	27.2	5.4	1.1	1.1	16.7
SAR–7443	Catatumbo	La Luna	2	73	1	0.4	0.5	6.2	1549.2	1.2	89.0	1421	13.9	177.1	46.9	34.6	17.1	1.6	0.8	26.2
CAB–115	Aguachica	La Luna	3	1909	<1	1.3	4.4	26.2	491.7	4.4	6.9	138	44.1	7.9	18.8	3.2	0.5	1.0	<0.1	2.0
QAD–50	Barichara	La Luna	7	2042	3	2.5	4.2	20.8	1182.2	7.4	36.6	115	100.7	7.0	17.5	2.6	0.8	0.8	<0.1	9.1
QLL–55	Catatumbo	La Luna	5	2390	2	0.3	0.6	6.0	2505.9	11.2	85.4	104	16.8	2.7	11.4	9.8	2.3	0.8	0.3	2.6
QAD–65	Barichara	La Luna	6	504	<1	0.3	1.0	7.1	1439.0	9.2	58.0	86	15.1	3.3	9.9	3.5	0.8	0.4	<0.1	2.8
QP–440	Villeta	Hilo	9	576	2	1.4	8.7	58.9	259.9	10.2	14.5	3865	61.4	163.1	59.2	45.1	11.8	1.7	1.7	34.4
O–05	CEOR	Hilo	16	1158	<1	3	10.4	119.1	79.0	11.7	55.6	2811	110.5	372.2	653.8	16.1	94.2	8.8	3.7	11.4
QP–435	Villeta	Hilo	7	567	<1	1.3	7.4	44.0	372.7	7.9	12.5	2535	55.0	121.0	33.4	52.2	18.4	1.3	1.9	45.2
QP–290	Villeta	Hilo	10	759	2	1.9	8.0	52.2	133.7	10.0	16.7	2205	59.7	108.2	53.1	57.5	7.6	2.1	2.3	37.4
O–15	CEOC	Hilo	13	1090	3	3.5	11.1	124.2	26.0	11.7	15.3	2033	121.4	97.8	824.7	16.5	15.8	6.9	0.6	9.9
O–40	CEOC	Hilo	16	595	2	3.6	11.6	146.5	18.6	12.7	16.0	2000	119.8	120.8	201.3	25.8	16.0	2.4	12.6	11.3
O–25	CEOC	Hilo	14	702	3	3.4	11.4	122.9	23.9	10.6	11.1	1576	117.5	75.6	48.0	48.2	21.7	1.9	1.8	79.3
O–45	CEOC	Hilo	15	556	<1	3.4	9.7	131.3	16.3	10.0	9.0	1296	109.0	60.6	101.5	120.6	38.1	2.7	3.0	74.1
C–12	CEOR	Macanal	29	194	2	5.2	10.9	75.8	101.0	8.6	2.0	94	187.9	1.0	60.3	15.5	<0.1	<0.1	<0.1	<0.5
MSP–25	CEOR	Macanal	24	453	4	7.1	23.6	242.8	28.2	12.2	3.9	182	231.1	1.2	55.0	16.2	2.2	<0.1	<0.1	0.5
COS14–459	Villa de Leyva	Villa de Leyva	23	265	3	2.9	10.6	137.6	286.4	10.7	5.4	272	144.1	7.6	19.8	11.5	0.8	<0.1	0.8	2.2
QED–35	CEOR	Fómeque	22	369	2	5.5	25.0	170.9	250.7	22.4	4.2	143	230.7	0.9	14.0	6.4	<0.1	<0.1	<0.1	<0.5
RSP–30	Villa de Leyva	Villa de Leyva	21	400	3	5.5	20.8	214.8	214.9	18.8	4.6	299	193.8	13.7	42.0	15.1	0.1	0.1	0.5	0.7
QED–00	CEOR	Fómeque	20	389	4	6.8	26.9	177.5	251.4	21.1	3.7	127	251.1	0.9	72.2	7.8	<0.1	<0.1	<0.1	<0.5
COS15–1553	Villa de Leyva	Paja	19	481	5	3.9	25.7	152.0	291.9	35.4	4.2	108	134.3	1.7	18.5	5.6	<0.1	<0.1	<0.1	<0.5
C–30	CEOR	Macanal	19	576	6	6.0	22.1	238.8	160.7	19.6	3.0	153	196.3	1.5	72.2	1.9	<0.1	<0.1	<0.1	<0.5
GA–60	CEOR	Macanal	17	528	9	6.6	20.6	193.7	137.4	17.2	4.2	181	220.9	14.9	20.9	10.9	0.2	<0.1	0.2	1.6
CON7–671	Villa de Leyva	San Gil Shale	13	270	7	11.8	33.4	91.6	237.2	31.9	5.4	56	416.3	1.3	11.7	8.1	<0.1	<0.1	<0.1	<0.5
RN–55	Villeta	Pacho	8	152	3	21.5	20.5	38.6	92.1	18.0	4.5	108	803.0	7.8	6.5	3.9	0.1	<0.1	0.3	1.0
CON6–674	Villa de Leyva	Churuvita	12	389	3	28.5	42.6	118.1	217.7	34.3	6.9	93	1058.1	1.6	7.1	8.7	<0.1	<0.1	0.1	<0.5
COS15–1739	Villa de Leyva	Paja	11	240	2	32.8	34.5	82.4	206.5	39.7	7.7	72	1232.4	1.0	19.0	15.5	0.2	<0.1	<0.1	<0.5
COS15–2054	Villa de Leyva	Paja	14	359	4	36.3	45.8	98.3	301.9	52.1	9.0	130	1336.5	2.9	13.2	14.6	0.1	<0.1	<0.1	<0.5

Murca Formation shales from the Tobia River (RT) of the Villeta area contain 6.5% dolomite and 3.9% ankerite. These two minerals have been reported as solid inclusions in emeralds (Pignatelli et al., 2015) and are associated with albite in hydrothermal veins and breccias that contain the emerald mineralization (Mantilla et al., 2008).

Mantle–derived Cretaceous gabbroic bodies were emplaced during the early extensional phases of the back–arc basin and

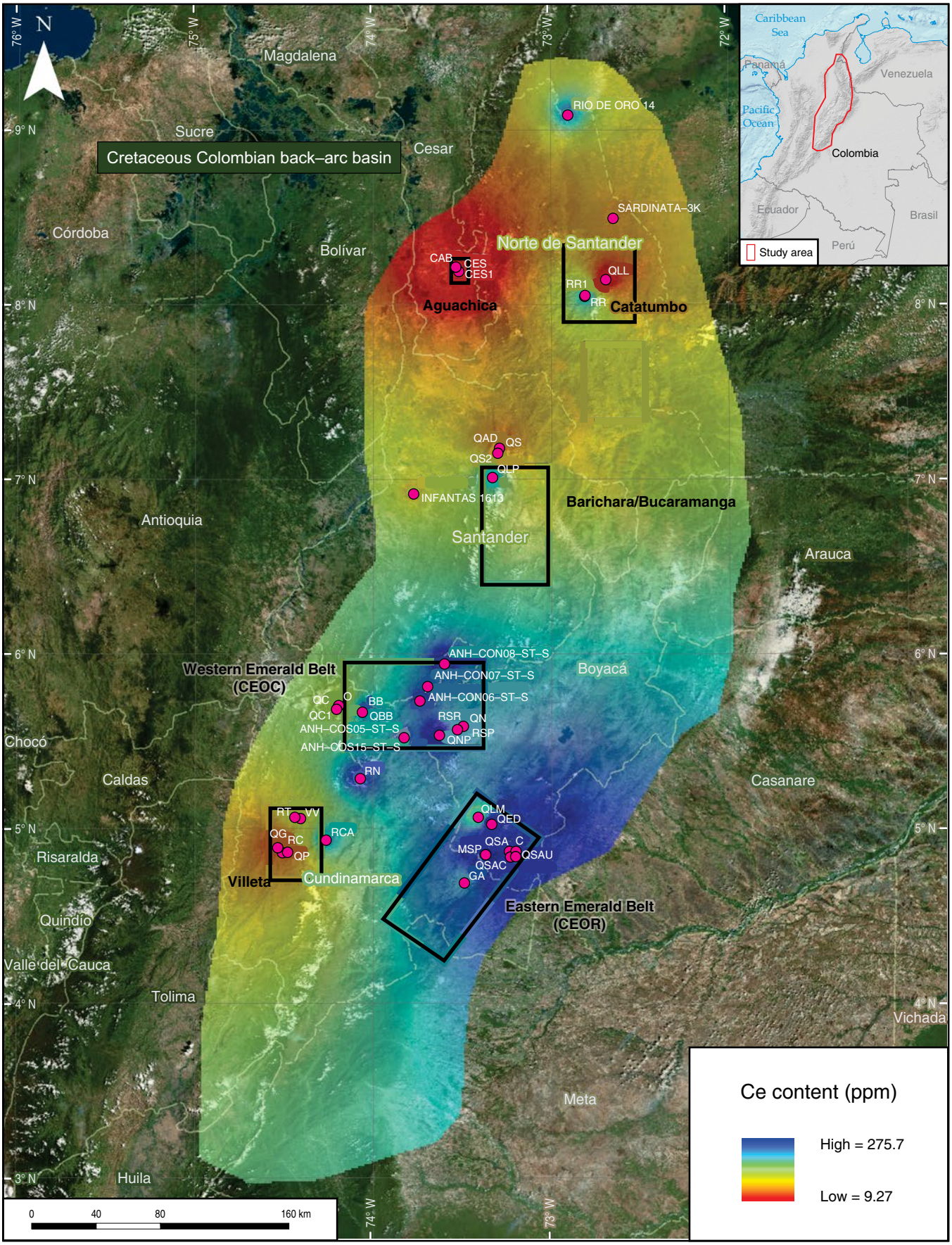

Figure 18. Cerium distribution from ICP–MS analyses. Values are average ppm per locality.

Table 9. Rare earth elements in ppm.

Sample	Area	Formation	Sc	Y	La	Ce	Pr	Nd	Sm	Eu	Gd	Tb	Dy	Ho	Er	Tm	Yb	Lu
COS14–1575	Villa de Leyva	Arcabuco	21	52.4	276.2	618.8	82.09	315.2	50.13	7.97	21.7	2.32	11.55	1.75	4.50	0.72	4.85	0.71
QBB–00	CEOC	Furatena	20	32.6	233.2	502.5	61.08	217.8	31.65	4.9	16.14	1.68	7.78	1.19	3.15	0.46	3.09	0.41
MSP–30	CEOR	Macanal	22	45.5	205.0	374.1	40.35	150.1	22.43	3.68	12.03	1.53	8.73	1.55	4.08	0.61	4.31	0.63
COS15–2054	Villa de Leyva	Paja	14	89.9	161.3	359.5	41.09	154.5	26.18	4.07	18.96	2.57	15.8	3.25	10.00	1.61	10.93	1.72
QSA–65	Villa de Leyva	Aguacaliente	12	104.5	118.7	299.3	35.17	133.8	25.49	4.30	22.58	3.59	19.18	3.32	8.71	1.17	6.96	1.01
COS15–1490	Villa de Leyva	Paja	13	38.6	119.8	287.6	30.62	109.9	17.09	2.70	12.33	1.52	7.64	1.46	4.08	0.62	4.12	0.62
O–75	CEOC	Hilo	12	52.9	142.1	233.0	29.09	99.8	11.24	1.67	7.51	0.78	4.36	1.14	3.96	0.59	4.00	0.68
MSP–35	CEOR	Macanal	21	43.3	119.3	214.9	23.72	88.6	15.19	2.71	10.64	1.57	8.39	1.72	4.82	0.68	4.57	0.65
CON7–485	Villa de Leyva	San Gil Shale	18	45.0	106.3	212.9	24.45	87.0	14.81	2.45	11.79	1.69	9.50	1.80	5.11	0.72	4.74	0.69
COS15–1360	Villa de Leyva	Paja	15	49.8	98.8	210.5	23.59	87.1	14.95	2.48	11.09	1.51	9.25	1.90	5.78	0.96	6.48	0.93
QSAU–18	Villa de Leyva	Une	19	39.7	95.6	199.2	21.95	76.5	13.28	2.25	10.08	1.51	8.32	1.55	4.46	0.68	4.37	0.68
CON6–1405	Villa de Leyva	Churuvita	19	45.6	94.9	198.3	22.50	83.2	15.32	2.60	12.97	1.91	9.88	1.83	4.66	0.70	4.35	0.67
CON7–1014	Villa de Leyva	San Gil Shale	20	41.2	101.2	198.0	22.80	80.1	13.42	2.28	9.77	1.26	7.60	1.55	4.94	0.73	4.62	0.70
QSAU–0	Villa de Leyva	Une	18	45.6	98.6	195.7	22.53	80.0	13.57	2.31	10.24	1.67	9.38	1.76	4.99	0.76	5.05	0.75
CON8–1958	Villa de Leyva	Paja	17	54.9	92.4	193.3	21.70	79.6	13.55	2.32	11.46	1.75	10.28	1.95	5.63	0.87	5.58	0.85
CON8–2025	Villa de Leyva	Paja	17	47.6	90.9	184.9	20.85	75.6	13.63	2.44	12.21	1.73	9.63	1.78	5.14	0.75	4.93	0.76
COS15–1739	Villa de Leyva	Paja	11	51.2	84.7	180.4	20.34	74.7	12.9	2.00	9.23	1.35	8.45	1.81	6.11	1.04	7.28	1.15
QS–00	Villa de Leyva	Salto	13	53.1	75.9	174.4	19.02	70.0	12.58	2.02	11.58	1.75	10.32	1.97	5.94	0.86	5.54	0.86
CON7–1655	Villa de Leyva	San Gil Shale	17	50.8	79.2	161.5	18.45	67.5	12.28	2.14	10.10	1.61	9.93	2.05	6.06	0.91	5.55	0.86
CON6–674	Villa de Leyva	Churuvita	12	54.6	74.1	158.4	17.60	63.6	9.91	1.47	7.08	1.22	8.33	1.92	6.00	1.05	7.19	1.14
COS15–1819	Villa de Leyva	Paja	13	47.4	79.1	156.7	18.05	66.5	11.96	1.96	9.86	1.36	8.09	1.64	4.97	0.82	5.78	0.90
CON8–1712	Villa de Leyva	Paja	15	48.5	72.9	147.8	16.59	61.0	11.39	2.11	10.49	1.63	9.25	1.80	5.21	0.81	5.38	0.85
QNP–00	Villa de Leyva	Paja	16	38.7	59.8	131.7	15.21	60.0	15.14	3.25	18.97	2.43	10.11	1.54	3.63	0.51	3.29	0.44
CON8–2296	Villa de Leyva	Paja	10	53.0	59.2	126.7	14.91	55.1	9.50	1.64	8.46	1.46	8.70	1.76	5.22	0.86	5.76	0.88
RN–40	Villa de Leyva	Pacho	12	41.1	52.3	105.0	13.08	50.8	11.13	2.13	12.03	1.68	8.51	1.56	4.46	0.63	4.39	0.64
O–85	CEOC	Hilo	21	29.1	46.7	90.0	13.01	52.4	15.12	3.34	12.44	1.81	9.62	1.66	4.29	0.59	3.82	0.49
QAD–50	Villa de Leyva	La Luna	7	130.0	67.7	88.3	11.81	44.1	8.26	1.58	9.12	1.6	10.71	2.54	8.15	1.19	7.78	1.19
QLL–55	Villa de Leyva	La Luna	5	223.7	97.2	75.7	15.15	64.0	12.80	3.13	17.18	2.52	16.16	3.89	12.09	1.66	10.25	1.73
C–12	CEOR	Macanal	29	29.0	31.6	63.8	7.65	30.8	6.65	1.23	6.42	0.99	4.88	1.09	3.32	0.43	3.19	0.47
QAD–65	Villa de Leyva	La Luna	6	168.6	73.2	61.2	11.06	44.4	9.73	2.27	12.73	1.89	11.47	2.80	8.65	1.25	7.62	1.25
COS14–459	Villa de Leyva	Villa de Leyva	23	20.7	28.8	56.6	7.03	28.0	5.90	1.72	5.84	0.83	4.19	0.74	2.16	0.33	2.36	0.36
VV–80	Villa de Leyva	Trincheras	10	50.5	29.8	55.7	6.57	26.6	4.96	1.14	7.23	1.37	8.11	1.89	4.73	0.66	3.92	0.55
RN–70	Villa de Leyva	Pacho	14	52.0	24.9	54.8	6.68	27.1	7.30	1.60	9.61	1.67	9.56	2.05	6.02	0.86	5.69	0.90
RT–10	Villa de Leyva	Murca	14	231.3	25.5	50.4	5.96	23.7	10.01	3.77	26.90	5.88	39.66	7.74	18.58	2.24	11.43	1.39
MSP–25	CEOR	Macanal	24	34.6	21.2	37.7	6.23	24.1	5.64	1.37	6.51	1.05	6.70	1.31	3.88	0.55	4.22	0.59

intruded Lower Cretaceous shales. These rocks include dikes of gabbro, diorite, and tonalite associated with hydrothermal activity that carried fluids related to the emerald mineralization. The ages reported by Vásquez et al. (2010) and the Radiometric Dating Catalog of Colombia, compiled by Gómez et al. (2015), indicate that the gabbros span Valanginian to Cenomanian time. The K–Ar and Ar–Ar ages from whole–rock and hornblende samples, which would reflect the ages of emplacement, are Valanginian to Hauterivian (Pacho), Barremian to Cenomanian (Cáceres), Aptian (Pajarito), Albian to Cenomanian (Rodrigoque), and Cenomanian (La Corona).

Vásquez et al. (2005, 2010) documented the geochemistry of the mafic to intermediate bodies, indicating tholeiitic affinity (MORB–like) from Cáceres and Pacho on the western side of the Eastern Cordillera and alkaline affinity (OIB–like) from Rodrigoque and Pajarito on the eastern side. The tonalite from La Corona in the western part of the Eastern Cordillera, near Cáceres and Pacho, also shows alkaline affinity. The authors

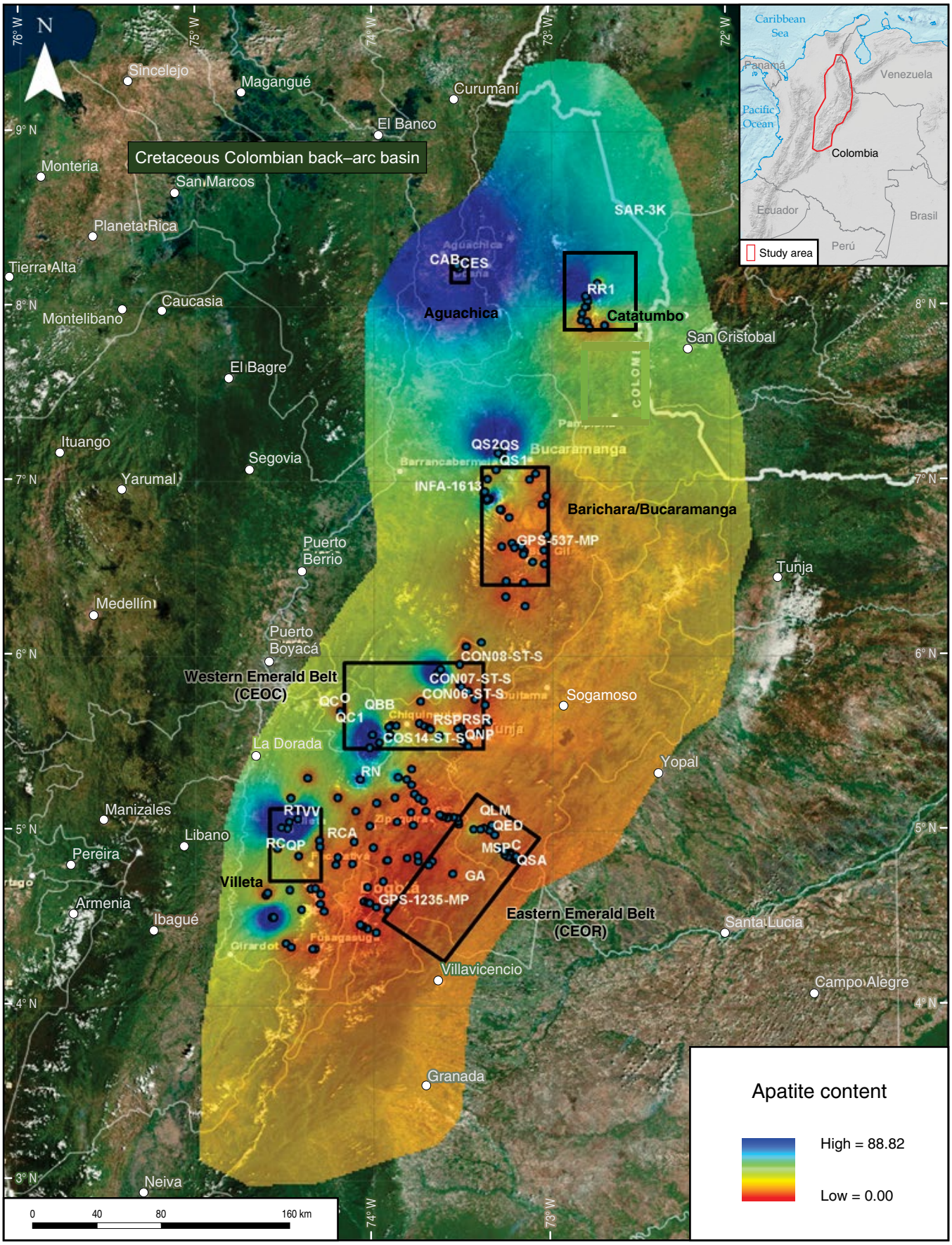

Figure 19. Regional distribution of apatite from heavy mineral analyses.

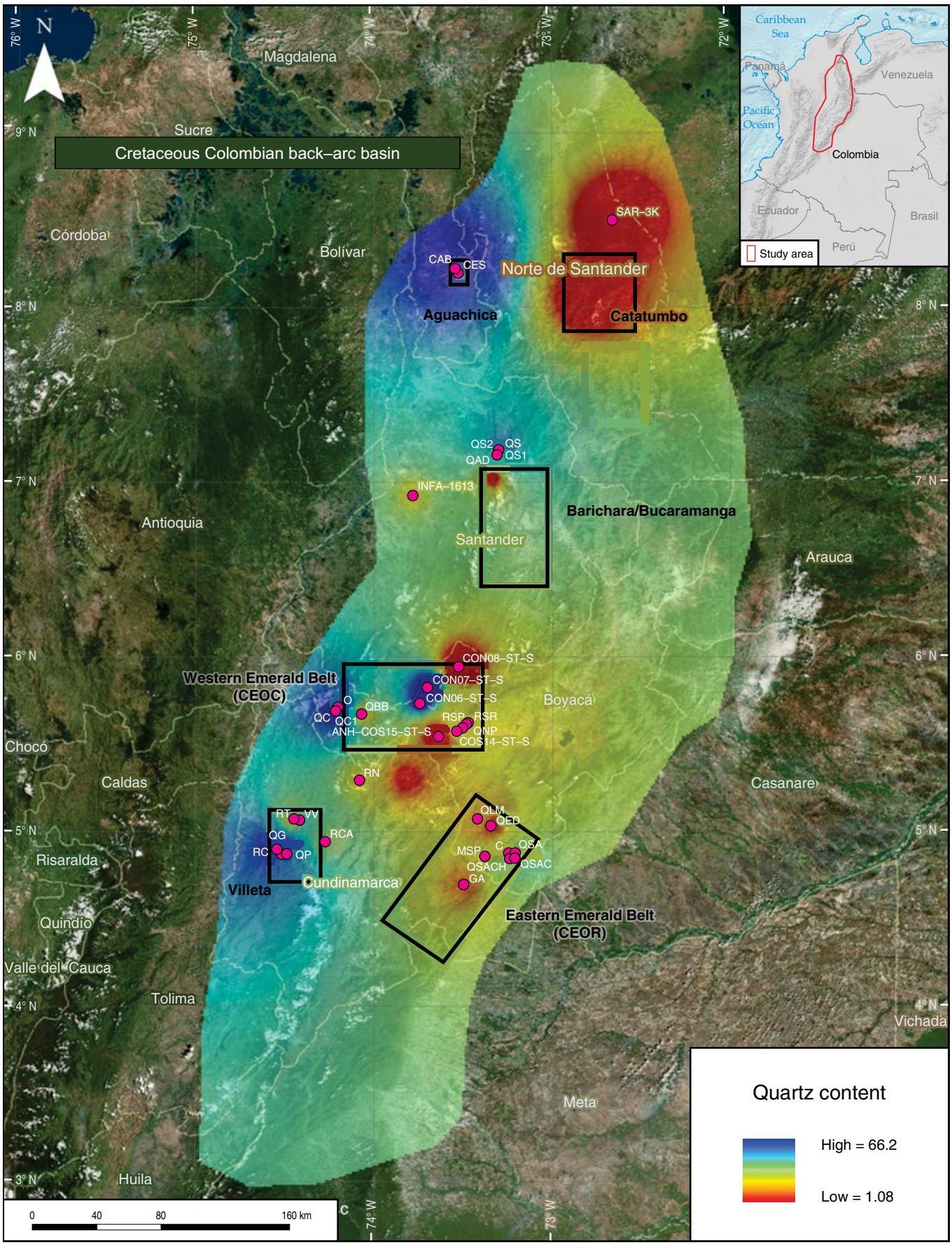

Figure 20. Quartz contents from XRD. Values plotted are average percentages per locality.

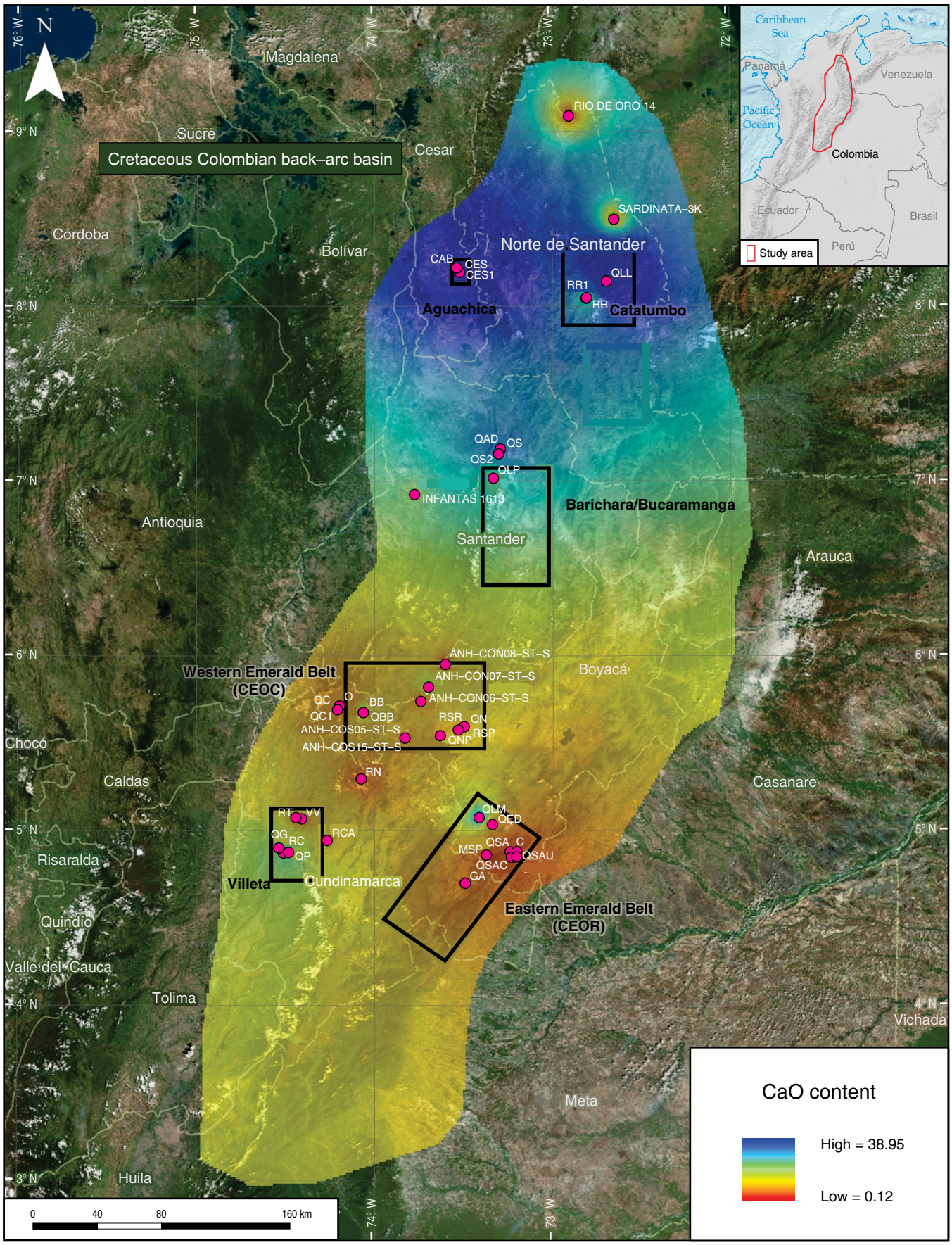

Figure 21. CaO contents from ICP–OES. Values plotted are average percentages per locality.

indicated a transition from a low to a high degree of partial melting and crustal contamination of mantle–derived magmas.

The wide range of muscovite K–Ar and Ar–Ar ages (Cheilletz et al., 1994, 1997; Gómez et al., 2015) of the mineralized emerald zones from the Macanal Formation: 76 ± 2.4 Ma to 58.4 ± 5.3 Ma (early Campanian to late Paleocene) and the Furatena Formation: 37.3 ± 0.1 Ma to 31.4 ± 0.3 Ma (late Eocene to early Oligocene), could indicate that not all the mineral systems were completely closed with respect to Ar due to the Early Cretaceous hydrothermal activity in the basin. For instance, the Cáceres Gabbro yields plagioclase Ar–Ar ages (Gómez et al., 2015; Vásquez et al. 2010) of 81.7 ± 0.8 Ma to 27 ± 1.9 Ma (early Campanian to late Oligocene), which are too young, considering the Early Cretaceous biostratigraphic ages of the strata intruded across the basin. The oldest whole–rock K–Ar age of the Cáceres Gabbro is 113.0 ± 16.0 Ma (early Barremian to early Cenomanian), which is closer to the age of emplacement. The Rodrigoque Gabbro presents the same situation; the youngest Ar–Ar age in plagioclase is 49.9 ± 0.2 Ma (early Eocene), but the oldest whole–rock K–Ar age is 106.5 ± 5.5 Ma (Albian). In the Corona Gabbro, the youngest Ar–Ar age in plagioclase is 64.3 ± 2.3 Ma (late Maastrichtian to Paleocene), but the oldest Ar–Ar age in hornblende is 97.8 ± 0.1 Ma (early Cenomanian). The muscovite and plagioclase ages younger than hornblende ages could indicate different closure temperatures, but the wide range of ages could also indicate argon loss during the Early Cretaceous hydrothermal activity, producing misleading younger ages.

We infer that the magmatic activity which affected the Lower Cretaceous strata in the basin produced several episodes of mineralization. The hydrothermal fluids that carried the scandium, vanadium, and beryllium were emplaced during Valanginian to Cenomanian rifting of the back–arc basin. Emeralds are present mostly in strata of Berriasian to Hauterivian age on both sides of the basin, so emerald mineralizing fluids must have been emplaced during the rifting stage when the basin experienced peak magmatic and hydrothermal activity. If the main mineralizing episode had occurred during the Cenozoic, then the emeralds would also have crystallized in younger strata and not primarily in Berriasian to Hauterivian shales. The Lower Cretaceous shales from the opposite eastern and western sides of the basin have different clay and REE signatures because of different source areas but share similar geochemical features because of the elements introduced during magmatic and hydrothermal activity.

Two other lines of evidence have been explored regarding the origin of emerald mineralization. One line is the maximum temperature reached by burial of the Berriasian to Hauterivian strata that host the main emerald mineralization, and the other line is the temperature of the mineralization itself. Silva et al. (2010) concluded that the chlorite (clinochlore) associated with the emerald mineralization hosted in Berriasian rocks with hydrothermal activity (which also contain hydrothermal albite and dolomite) crystallized at ca. 354 °C and that such a temperature was consistent with the temperature (ca. 335 °C) of fluid inclusions in the emeralds reported by Mantilla et al. (2008). On the other hand, Mora et al. (2013) established that cleavage was produced at maximum paleotemperatures (ca. 220 °C deduced from ZFT and vitrinite reflectance) during the late Oligocene; fold–related calcite–filled veins and late stages of cleavage were produced at temperatures between 220 °C and 160 °C during the early Miocene, indicating that the strata accumulated strain for a few million years before first–order thrusting, which was produced during the late Miocene and Pliocene uplift of the Eastern Cordillera. The temperatures obtained from the two data sets were attained during different events: One temperature (ca. 354 °C) is that of chlorite and emerald mineralization during Valanginian to Cenomanian hydrothermal activity, and the other temperature (220 to 160 °C) represents the maximum burial at which the strata began accumulating strain before thrust movement occurred during late Miocene uplift.

We postulate that at a micro scale, the normal faults and extensional fractures that controlled the basin during the Early Cretaceous were the main conduits for the hydrothermal fluids that formed the emeralds. Many but not all of these normal faults and fracture planes were later inverted during the Miocene thrusting and uplifting of the basin. For instance, Mantilla et al. (2008) indicate that in the Oriente mine of the CEOR, fragments of hydrothermal veins with emeralds are present in fractures produced during a recent tectonic event that destroyed the emerald mineralization. Mora et al. (2013) indicated that most of the planar fabrics, veins, and fractures are correlated with the main folds that affected the Cretaceous rocks during the late Oligocene and early Miocene, but in the mining area of El Porvenir in the Gachalá dome, orthogonal veins filled with calcite have no parallelism or symmetry with any contractional fold.

Since there are no igneous bodies of Campanian to Oligocene age intruding the strata of the basin, which could support the hypothesis of hydrothermal activity during this time span, and since the temperature produced by burial diagenesis was not high enough (less than 220 °C for the oldest strata), we prefer the interpretation of emerald mineralization during Early Cretaceous hydrothermal activity with temperatures higher than 350 °C.

5. Conclusions

Detrital zircon U–Pb ages document two source areas for the back–arc Cretaceous Colombian Basin. One source on the E side of the basin has Archean, Proterozoic, and Paleozoic ages derived from the Guiana Shield, and the other source on the W side of the basin has Triassic to Cretaceous ages, including very abundant Jurassic particles derived from the Central Cordillera magmatic arc. Other important particles derived from the Central Cordillera have Paleozoic ages, along with a small number of Proterozoic particles. No Mesozoic particles are present in the samples from the E side of the Eastern Cordillera.

The fluvial system of Berriasian to Valanginian age that deposited the Tambor Formation and time–equivalent fluvial units in the center of the basin contained particles sourced from both the E and W sides of the basin, including distributary streams feeding a trunk river flowing northward to the Caribbean. The central rift of the basin was completely flooded during the late Valanginian, as indicated by the offshore shales, marlstones, and biomicrites deposited in large areas of Cundinamarca, Boyacá, and Santander Departments. The horsts that separated the early grabens of the basin were definitely covered during the late Valanginian. After this time, the Cretaceous seaway was separated into two shorelines supplied from E and W sources on opposite sides of the basin. Fluvial environments during the rest of Cretaceous time were also separated on the opposite E and W margins of the basin. No mixing of particles from opposite E and W source areas or from local horsts occurred in the basin after the Valanginian.

XRD analyses show that black shale mudstones of the basin are composed mainly of clay minerals and quartz silt. The highest contents of kaolinite (50 to 55 %) are from the Paja Formation in the Santander area and the Une and Chipaque Formations in the Llanos Foothills, both sourced from the Guiana Shield. The highest average illite contents (60 to 65 %) are from shales of the Simití and El Salto Formations in the Infantas well and from the Hilo Formation in the Otanche section; both are situated toward the W side of the basin. Chlorite is present in minor amounts compared to kaolinite and illite; the highest average percentage of chlorite (22%) comes from the lower part of the Murca Formation in the Tobia River section of the Villeta area. Chlorite was derived from low–grade metamorphic rocks sourced from the Central Cordillera.

ICP–MS analyses reveal several important elements associated with the clay content of black shales from the basin, which also help to discriminate between eastern and western sources. The highest contents of titanium, zirconium, thorium, niobium, hafnium, and tantalum in the study come from a shale sample of the Paja Formation in the Villa de Leyva area. The unit was sourced from the eastern side of the basin, which has more differentiated continental crust than the western sources. In contrast, the highest contents of chromium, copper, molybdenum, arsenic, antimony, selenium, thallium, and silver in the study come from the shales of the Hilo Formation in the Otanche section, which also have very high contents of illite. This unit was sourced from the western side of the basin, which included the magmatic/metamorphic arc and accreted oceanic crust.

The light REE of the cerium group have the maximum values for this study in a siltstone sample from the upper part of the Arcabuco Formation in the ANH COS–14 well in the vicinity of Villa de Leyva. In contrast, the heavy REE of the yttrium group have the maximum values for this study in a sample from the lower part of the Murca Formation in the Tobia River section. The high contents of the yttrium group indicate an ultramafic source in accreted oceanic crust along the western basin margin, while the cerium group indicates more differentiated continental crust on the eastern basin margin.

Another important mineral that indicates provenance is apatite, which shows higher percentages in the western part of the basin and is related to igneous and metamorphic sources in the Central Cordillera. Samples with heavy mineral analyses containing high percentages of terrigenous apatite come from the Murca, Trincheras, Socotá, Hilo, and Pacho Formations in the Villeta area. Another important fraction of the reported apatite is related to phosphatic biomicrites and has an authigenic origin because of biological accumulation in fish. The highest percentages of fluorapatite from XRD analyses are from La Luna Formation. The highest contents of uranium in the study are associated with the biologically concentrated phosphates of La Luna Formation.

The highest calcium (CaO) contents (40 to 55 %), obtained from ICP–OES analyses, come from the biomicrite limestones of La Luna Formation on the W and N sides of the basin. The highest contents of SiO_2 (59 to 79 %) in diagenetic cherts are also from La Luna Formation, in addition to the Lidita Inferior and Lidita Superior Formations, Hilo Formation, and La Frontera Member of the Conejo Formation.

Mantle–derived gabbroic to intermediate bodies emplaced during the early extensional synrift phase of the back–arc basin intruded Lower Cretaceous shales. The former rocks include dikes of gabbro, diorite, and tonalite, associated with important hydrothermal activity that carried the fluids that produced the emerald mineralization. The highest values of scandium are found in shales of the CEOR, whereas the highest values of vanadium are present in shales of the CEOC. The wide range of muscovite and plagioclase ages from the mineralized emerald zones (early Campanian to late Oligocene), much younger than the hornblende and whole–rock ages of emplacement of the gabbros (Valanginian to Cenomanian), might indicate that the systems were not closed with respect to Ar, producing misleading younger ages. Argon loss could be due to several factors, including Early Cretaceous hydrothermal activity, increasing temperature during Late Cretaceous to Oligocene sedimentation, and compressional strain during Miocene uplift of the Eastern Cordillera. There are no igneous bodies or other known sources of heat, which could support the hypothesis of hydrothermal activity during the Campanian to Oligocene.

Acknowledgments

We thank the Agencia Nacional de Hidrocarburos for permission to publish their data. The field work and analyses were conducted within project 299–12 to evaluate the unconventional hydrocarbon potential of fine–grained strata from the Cretaceous Colombian Basin. The project was directed by Javier GUERRERO and supervised by Alejandra MEJÍA–MOLINA.

We also thank Dr. Brian HORTON from the University of Texas, Dr. Andres MORA from ICP, and an anonymous reviewer for valuable suggestions that helped us improve the paper.

References

Barham, M., Kirkland, C.L., Reynolds, S., O'Leary, M.J., Evans, N.J., Allen, H., Haines, P.W., Hocking, R.M., McDonald, B.J., Belousova, E. & Goodall, J. 2016. The answers are blowin' in the wind: Ultra–distal ashfall zircons, indicators of Cretaceous super–eruptions in eastern Gondwana. Geology, 44 (8): 643–646. https://doi.org/10.1130/G38000.1

Bonilla, G.E., Sarmiento, G.A. & Gaviria, S. 2011. Proveniencia y transformación diagenética de minerales arcillosos del Maastrichtiano–Paleoceno al norte de Bogotá, cordillera Oriental de Colombia. Geología Colombiana, 36(1): 179–196.

Bustamante, C., Cardona, A., Bayona, G., Mora, A., Valencia, V., Gehrels, G. & Vervoort, J. 2010. U–Pb LA–ICP–MS geochronology and regional correlation of Middle Jurassic intrusive rocks from the Garzón Massif, Upper Magdalena Valley and Central Cordillera, southern Colombia. Boletín de Geología, 32(2): 93–109.

Cheilletz, A., Féraud, G., Giuliani, G. & Rodriguez, C.T. 1994. Time–pressure and temperature constraints on the formation of Colombian emeralds: An $^{40}Ar/^{39}Ar$ laser microprobe and fluid inclusion study. Economic Geology, 89(2): 361–380. https://doi.org/10.2113/gsecongeo.89.2.361

Cheilletz, A., Giuliani, G., Branquet, Y., Laumonier, B., Sanchez, A.J., Féraud, G. & Arhan, T. 1997. Datation K–Ar et $^{40}Ar/^{39}Ar$ à 65 + 3 Ma des gisements d'émeraude du district de Chivor–Macanal: Argument en faveur d'une déformation précoce dans la Cordillère Orientale de Colombie. Comptes–Rendus de l'Académie des Sciences, 324(5): 369–377. Paris, France.

Chew, D.M. & Donelick, R.A. 2012. Combined apatite fission track and U–Pb dating by LA–ICP–MS and its application in apatite provenance analysis. Mineralogical Association of Canada, Short Course 42: 219–247.

Clavijo, J., Mantilla, L., Pinto, J., Bernal, L. & Pérez, A. 2008. Evolución geológica de la serranía de San Lucas, norte del Valle Medio del Magdalena y noroeste de la cordillera Oriental. Boletín de Geología, 30(1): 45–62.

Cooper, M.A., Addison, F.T., Álvarez, R., Coral, M., Graham, R.H., Hayward, A.B., Howe, S., Martínez, J., Naar, J., Peñas, R., Pulham, A.J. & Taborda, A. 1995. Basin development and tectonic history of the Llanos Basin, Eastern Cordillera, and Middle Magdalena Valley, Colombia. American Association of Petroleum Geologists Bulletin, 79(10): 1421–1443.

Etayo–Serna, F., De Porta, N.S., De Porta, J. & Gaona, T. 2003. The Batá Formation of Colombia is truly Cretaceous, not Jurassic. Journal of South American Earth Sciences, 16(3): 113–117. https://doi.org/10.1016/S0895-9811(03)00048-8

Gómez, J., Montes, N.E., Alcárcel, F.A. & Ceballos, J.A. 2015. Catálogo de dataciones radiométricas de Colombia en ArcGIS y Google Earth. In: Gómez, J. & Almanza, M.F. (editors), Compilando la geología de Colombia: Una visión a 2015. Servicio Geológico Colombiano, Publicaciones Geológicas Especiales 33, p. 63–419. Bogotá.

Guerrero, J. 2002a. A proposal on the classification of systems tracts: Application to the allostratigraphy and sequence stratigraphy of the Cretaceous Colombian Basin. Part 1: Berriasian to Hauterivian. Geología Colombiana, (27): 3–25.

Guerrero, J. 2002b. A proposal on the classification of systems tracts: Application to the allostratigraphy and sequence stratigraphy of the Cretaceous Colombian Basin. Part 2: Barremian to Maastrichtian. Geología Colombiana, (27): 27–49.

Guerrero, J. & Sarmiento, G. 1996. Estratigrafía física, palinológica, sedimentológica y secuencial del Cretácico Superior y Paleoceno del Piedemonte Llanero: Implicaciones en exploración petrolera. Geología Colombiana, 20: 3–66.

Guerrero, J., Sarmiento, G. & Navarrete, R. 2000. The stratigraphy of the W side of the Cretaceous Colombian Basin in the Upper Magdalena Valley. Reevaluation of selected areas and type localities including Aipe, Guaduas, Ortega, and Piedras. Geología Colombiana, (25): 45–110.

Hettner, A. 1892. Die Kordillere von Bogotá. Gotha: Justus Perthes, 131 p.

Horton, B.K., Saylor, J.E., Nie, J., Mora, A., Parra, M., Reyes–Harker, A. & Stockli, D.F. 2010. Linking sedimentation in the northern Andes to basement configuration, Mesozoic extension, and Cenozoic shortening: Evidence from detrital zircon U–Pb ages, Eastern Cordillera, Colombia. Geological Society of America Bulletin, 122(9–10): 1423–1442. https://doi.org/10.1130/B30118.1

Horton, B.K., Anderson, V.J., Caballero, V., Saylor, J.E., Nie, J., Parra, M. & Mora, A. 2015. Application of detrital zircon U–Pb geochronology to surface and subsurface correlations of provenance, paleodrainage and tectonics of the Middle Magdalena Valley Basin of Colombia. Geosphere, 11(6): 1790–1811. https://doi.org/10.1130/GES01251.1

Mantilla, L.C., Silva, A., Conde, J., Gaviria, J.A., Gallo, F.H., Torres, D.A., Ortegon, J.M., Silva, E.N., Tarazona, C.A., Castro, B.J. & Garcia, C.A. 2008. Estudio de los procesos de interacción fluido–roca en el cinturón esmeraldífero oriental (cordillera Oriental, Colombia) y su importancia en la exploración de nuevos yacimientos hidrotermales. Ingeominas–Universidad Industrial de Santander, unpublished report, 496 p. Bogotá.

Moore, T.E. 2014. U–Pb zircon age data for selected sedimentary, metasedimentary, and igneous rocks from northern and central Alaska. U.S. Geological Survey Data Series 899, 4 p. https://doi.org/10.3133/ds899

Moore, T.E., O'Sullivan, P.B., Potter, C.J. & Donelick, R.A. 2015. Provenance and detrital zircon geochronologic evolution of lower Brookian foreland basin deposits of the western Brooks Range,

Alaska, and implications for early Brookian tectonism. Geosphere, 11(1): 93–122. https://doi.org/10.1130/GES01043.1

Mora, A., Horton, B.K., Mesa, A., Rubiano, J., Ketcham, R.A., Parra, M., Blanco, V., Garcia, D. & Stockli, D.F. 2010. Migration of Cenozoic deformation in the Eastern Cordillera of Colombia interpreted from fission track results and structural relationships: Implications for petroleum systems. American Association of Petroleum Geologists Bulletin, 94(10): 1543–1580. https://doi.org/10.1306/01051009111

Mora, A., Blanco, V., Naranjo, J., Sanchez, N., Ketcham, R.A., Rubiano, J., Stockli, D.F., Quintero, I., Nemčok, M., Horton, B.K. & Davila, H. 2013. On the lag time between internal strain and basement involved thrust induced exhumation: The case of the Colombian Eastern Cordillera. Journal of Structural Geology, 52: 96–118. https://doi.org/10.1016/j.jsg.2013.04.001

Moreno, J.M. 1990. Stratigraphy of the Lower Cretaceous Rosablanca and Cumbre Formations, Útica Sandstone and Murca Formation, west flank, Eastern Cordillera, Colombia. Geología Colombiana, 17: 65–86.

Moreno, J.M. 1991. Provenance of the Lower Cretaceous sedimentary sequences, central part, Eastern Cordillera, Colombia. Revista de la Academia Colombiana de Ciencias Exactas, Físicas y Naturales, 18(69): 159–173.

Ordóñez–Carmona, O., Restrepo, J.J. & Pimentel, M.M. 2006. Geochronological and isotopical review of pre–Devonian crustal basement of the Colombian Andes. Journal of South American Earth Sciences, 21(4): 372–382. https://doi.org/10.1016/j.jsames.2006.07.005

Pignatelli, I., Giuliani, G., Ohnenstetter, D., Agrosi, G., Mathieu, S., Morlot, C. & Branquet, Y. 2015. Colombian trapiche emeralds: Recent advances in understanding their formation. Gems & Gemology, 51(3): 222–259. http://dx.doi.org/10.5741/GEMS.51.3.222

Restrepo–Pace, P.A., Ruiz, J., Gehrels, G. & Cosca, M. 1997. Geochronology and Nd isotopic data of Grenville–age rocks in the Colombian Andes: New constraints for late Proterozoic – early Paleozoic paleocontinental reconstructions of the Americas. Earth and Planetary Science Letters, 150(3–4): 427–441. https://doi.org/10.1016/S0012-821X(97)00091-5

Sarmiento–Rojas, L.F., van Wess, J.D. & Cloetingh, S. 2006. Mesozoic transtensional basin history of the Eastern Cordillera, Colombian Andes: Inferences from tectonic models. Journal of South American Earth Sciences, 21(4): 383–411. https://doi.org/10.1016/j.jsames.2006.07.003

Silva, A., Mantilla, L.C., Terraza, R. 2010. Clasificación química y geotermometría de las cloritas de las formaciones cretácicas Santa Rosa y Lutitas de Macanal, cinturón esmeraldífero oriental, cordillera Oriental, Colombia. Boletín de Geología, 32 (2): 45–54.

Smith, J.J., Turner, E., Möller, A., Joeckel, R.M. & Otto, R.E. 2018. First U–Pb zircon ages for late Miocene Ashfall Konservat–Lagerstätte and Grove Lake ashes from eastern Great Plains, USA. PLOS ONE 13(11): e0207103. https://doi.org/10.1371/journal.pone.0207103

Stacey, J.S. & Kramers, J.D. 1975. Approximation of terrestrial lead isotope evolution by a two–stage model. Earth and Planetary Science Letters, 26(2): 207–221. https://doi.org/10.1016/0012-821X(75)90088-6

Steiger, R.H. & Jäger, E. 1977. Subcommission on geochronology: Convention on the use of decay constants in geo– and cosmochronology. Earth and Planetary Science Letters, 36(3): 359–362. https://doi.org/10.1016/0012-821X(77)90060-7

Tesón, E., Mora, A., Silva, A., Namson, J., Teixell, A., Castellanos, J., Casallas, W., Julivert, M., Taylor, M., Ibañez–Mejia, M. & Valencia, V. 2013. Relationship of Mesozoic graben development, stress, shortening magnitude, and structural style in the Eastern Cordillera of the Colombian Andes. In: Nemčok, M., Mora, A. & Cosgrove, J.W. (editors), Thick–skin–dominated orogens: From initial inversion to full accretion. Geological Society of London, Special Publication 377, p. 257–283. London. https://doi.org/10.1144/SP377.10

Vásquez, M., Altenberger, U., Romer, R.L. & Moreno, J.M. 2005. Extension–related magmatism during mid–Cretaceous times in the Eastern Cordillera, Colombia. 6th International Symposium on Andean Geodynamics, Extended Abstracts, p. 770–772. Barcelona, Spain.

Vásquez, M., Altenberger, U., Romer, R.L., Sudo, M. & Moreno–Murillo, J.M. 2010. Magmatic evolution of the Andean Eastern Cordillera of Colombia during the Cretaceous: Influence of previous tectonic processes. Journal of South American Earth Sciences, 29(2): 171–186. https://doi.org/10.1016/j.jsames.2009.02.003

Vesga, C.J. & Barrero, D. 1978. Edades K/Ar en rocas ígneas y metamórficas de la cordillera Central de Colombia y su implicación geológica. II Congreso Colombiano de Geología. Abstracts, p. 19. Bogotá.

Villagómez, D., Spikings, R., Magna, T., Kammer, A., Winkler, W. & Beltrán, A. 2011. Geochronology, geochemistry and tectonic evolution of the Western and Central Cordilleras of Colombia. Lithos, 125(3–4): 875–896. https://doi.org/10.1016/j.lithos.2011.05.003

Zapata, S., Cardona, A., Jaramillo, C., Valencia, V. & Vervoort, J. 2016. U–Pb LA–ICP–MS geochronology and geochemistry of Jurassic volcanic and plutonic rocks from the Putumayo region (southern Colombia): Tectonic setting and regional correlations. Boletín de Geología, 38(2): 1–38. https://doi.org/10.18273/revbol.v38n2-2016001

Explanation of Acronyms, Abbreviations, and Symbols:

ANH	Agencia Nacional de Hidrocarburos
CEOC	Western Emerald Belt
CEOR	Eastern Emerald Belt
ICP–MS	Inductively coupled plasma mass spectrometry
ICP–OES	Inductively coupled plasma optical emission spectrometry
LA–ICP–MS	Laser ablation inductively coupled plasma mass spectrometry
LOI	Loss on ignition
MMV	Middle Magdalena Valley
MORB	Mid–ocean ridge basalt
OIB	Ocean island basalt
REE	Rare earth element
UMV	Upper Magdalena Valley
XRD	X–ray powder diffraction
ZFT	Zircon fission track

Authors' Biographical Notes

Javier GUERRERO is a geologist from the Universidad Nacional de Colombia. He obtained a Master of Science degree and a PhD from Duke University (USA) in the areas of stratigraphy, sedimentology, and paleomagnetism. He participated with a multidisciplinary group of geologists and paleontologists from several American universities in a project on biostratigraphy, sedimentology, and magnetostratigraphy of the Honda Group in the Tatacoa Desert. He worked at the stratigraphy section of the Servicio Geológico Colombiano on various projects on the Cenozoic from the Magdalena River Valley. Recently, he has been a professor in the Departamento de Geociencias at the Universidad Nacional de Colombia, lecturing in courses on sedimentology, sequence stratigraphy, and regional geology. Javier has conducted research and consulting projects for several petroleum companies and for the Agencia Nacional de Hidrocarburos (ANH) on rocks of the Cretaceous Colombian back–arc basin and the Cenozoic foreland basin.

Alejandra MEJÍA–MOLINA is a geologist from the Universidad de Caldas (Colombia) who has been working during the last decade in paleontology, paleoecology, paleoceanography, and paleoclimatology as a member of the Grupo de Geociencias Oceánicas (GGO) at the Universidad de Salamanca (España). Her Master's thesis was on Quaternary marine/continental variability in North Africa and her Doctoral thesis was on calcareous nannofossils, both at the Universidad de Salamanca. Alejandra worked for the Agencia Nacional de Hidrocarburos (ANH) on several projects to obtain new geological data and evaluate the Colombian exploratory potential of both conventional (Pacific and Caribbean offshore basins) and unconventional hydrocarbons (Cretaceous from the Eastern Cordillera). She currently works for the Escuela de Ciencias Geológicas e Ingeniería at the Universidad Yachay Tech, Ecuador.

José OSORNO is a geologist from the Universidad de Caldas with a specialization in project management from the Universidad Piloto de Colombia. He recently completed a Master of Science in energy management at Universidad Sergio Arboleda and an Executive MBA at the Universitat Politècnica de València, España. José Fernando worked for 18 years at the Servicio Geológico Colombiano in the División de Geología Regional y Estratigrafía. Recently, he has been working at the Agencia Nacional de Hidrocarburos (ANH) in project design and evaluation, including the definition of oil systems in Colombia and geochemical evaluation of the Sinú–San Jacinto area. He is currently responsible for "yet–to–find" projects focused on calculating the potential of hydrocarbons yet to be discovered in the sedimentary basins of Colombia. José is also responsible for projects on the potential of unconventional hydrocarbons in the country.